British Geological Survey

Petrography and Diagenesis of the Bunter Sandstone Formation in the UK Southern North Sea

DRM Programme

Open Report OR/23/054

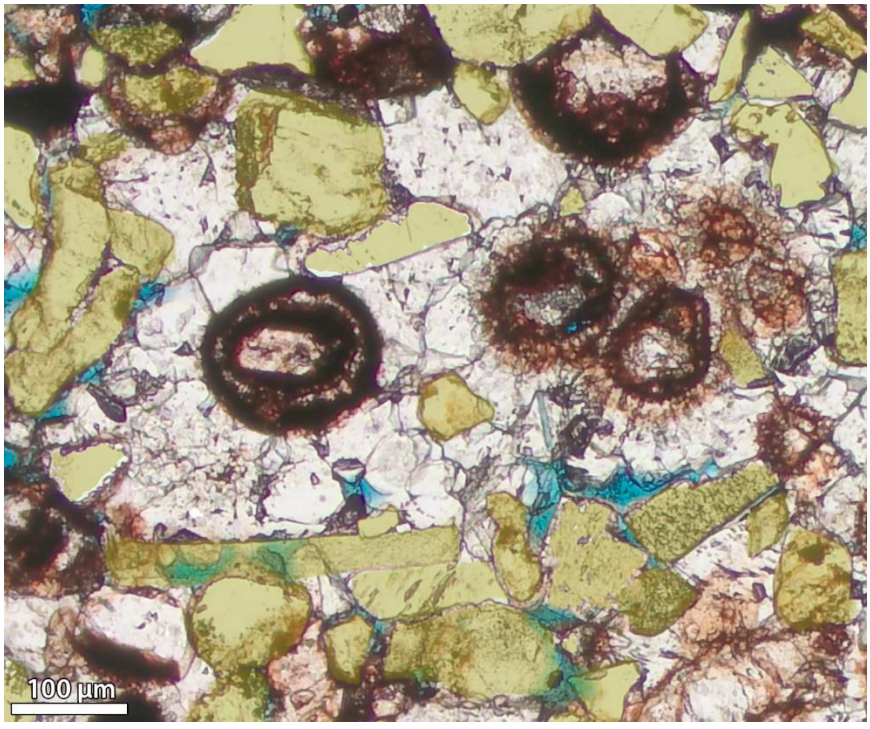

BRITISH GEOLOGICAL SURVEY

DRM PROGRAMME

OPEN REPORT OR/23/054

Petrography and Diagenesis of the Bunter Sandstone Formation in the UK Southern North Sea

J C Rushton, S Hannis and A E Milodowski

Contributor/editor

J Williams

Keywords

Diagenesis; Calcrete; Dolocrete; Halite; Nodules; Bunter Sandstone Formation; UK Southern North Sea.

Front cover

Optical PPL from a mm-thick calcrete lamination with abundant calcite nodules, showing their characteristic hematitic clay bands and a wide range of shapes and forms. Hematite-stained stellate outers (right of centre) are amongst features that indicate at least some *in situ* growth. A yellow AQM-derived overlay of detrital silicate grains highlights their widespread displacement by nodule-centred eodiagenetic calcite cement. Blue-dyed resin highlights remnant porosity. 1142.5 m, 42/25-1.

Bibliographical reference

RUSHTON, J C, HANNIS, S, MILODOWSKI, A E. 2023. Petrography and Diagenesis of the Bunter Sandstone Formation in the UK Southern North Sea. *British Geological Survey Open Report*, OR/23/054. 59pp.

Keyworth, Nottingham British Geological Survey 2023

BRITISH GEOLOGICAL SURVEY

The full range of our publications is available from BGS shops at Nottingham, Edinburgh, London and Cardiff (Welsh publications only) see contact details below or shop online at www.geologyshop.com

The London Information Office also maintains a reference collection of BGS publications, including maps, for consultation.

We publish an annual catalogue of our maps and other publications; this catalogue is available online or from any of the BGS shops.

The British Geological Survey carries out the geological survey of Great Britain and Northern Ireland (the latter as an agency service for the government of Northern Ireland), and of the surrounding continental shelf, as well as basic research projects. It also undertakes programmes of technical aid in geology in developing countries.

The British Geological Survey is a component body of UK Research and Innovation.

British Geological Survey offices

Nicker Hill, Keyworth,
Nottingham NG12 5GG

Tel 0115 936 3100

BGS Central Enquiries Desk

Tel 0115 936 3143
email enquiries@bgs.ac.uk

BGS Sales

Tel 0115 936 3241
email sales@bgs.ac.uk

The Lyell Centre, Research Avenue South,
Edinburgh EH14 4AP

Tel 0131 667 1000
email scotsales@bgs.ac.uk

Natural History Museum, Cromwell Road,
London SW7 5BD

Tel 020 7589 4090
Tel 020 7942 5344/45
email bgslondon@bgs.ac.uk

Cardiff University, Main Building, Park Place,
Cardiff CF10 3AT

Tel 029 2167 4280

Maclean Building, Crowmarsh Gifford,
Wallingford OX10 8BB

Tel 01491 838800

Geological Survey of Northern Ireland, Department of Enterprise, Trade & Investment, Dundonald House, Upper Newtownards Road, Ballymiscaw,
Belfast, BT4 3SB

Tel 01232 666595
www.bgs.ac.uk/gsni/

Natural Environment Research Council, Polaris House,
North Star Avenue, Swindon SN2 1EU

Tel 01793 411500 Fax 01793 411501
www.nerc.ac.uk

UK Research and Innovation, Polaris House,
Swindon SN2 1FL

Tel 01793 444000
www.ukri.org

Website www.bgs.ac.uk
Shop online at www.geologyshop.com

Contents

FIGURES

TABLES

Summary

This report describes a regional petrographic study of the Triassic aged Bunter Sandstone Formation (BSF) in the northern part of the UK Southern North Sea. To date, the spatial relationships leading to the prediction of regional reservoir quality in the BSF in terms of its potential for storage of CO_2 or hydrogen have not been fully understood. Previous studies have been largely focused on the hydrocarbon fields and these have shown that the presence or absence of diagenetic cements can both create barriers and enhance pathways for fluid flow. More recent studies investigating CO_2 storage potential through regional dynamic modelling have demonstrated the importance of physical and chemical property distributions. This applies not only to the immediate injection and containment of the CO_2 plume but also to the impacts of the pressure footprints created from injecting a large volume of fluid and the potential interaction between neighbouring sites. However, a consensus allowing an extrapolation of reservoir quality prediction to the more data-poor saline aquifer parts of the BSF has not proved straightforward as evidenced by results of a CO_2 storage exploration well drilled in 2010. This has highlighted the importance of improving regional understanding of reservoir storage potential for future CO_2 or hydrogen appraisal activities. This report adds to the body of research attempting to discern reservoir rock property distribution in the BSF through detailed petrographic observations to understand their diagenetic histories through the analysis of 83 samples across 12 wells. Diagenetic observations are described and presented as a proposed diagenetic history in the figure below.

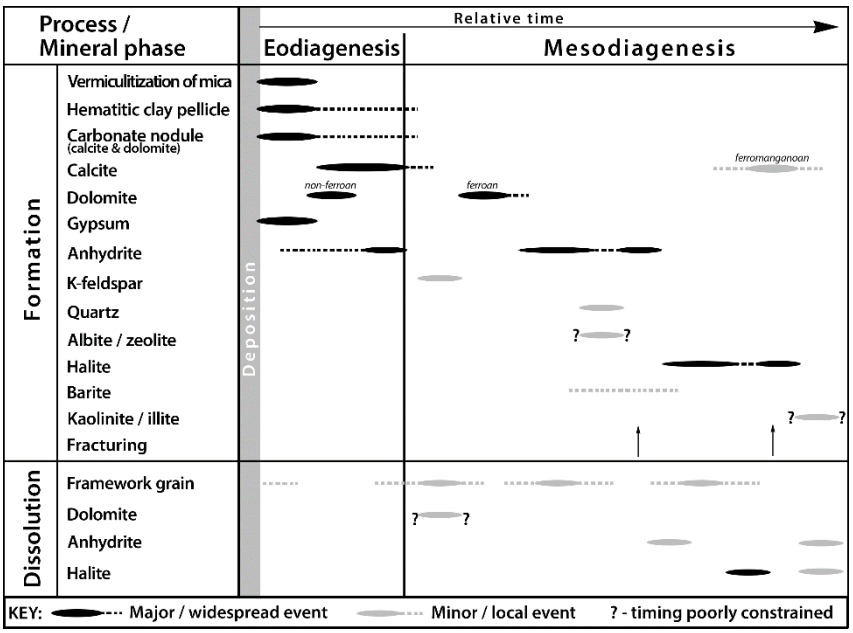

Detrital and near-surface diagenesis (eodiagenetic) characteristics of the BSF are consistent with terrestrial deposition under arid conditions, principally with fluvial origins and a minor aeolian input. The eodiagenetic phases that are particularly characteristic of arid conditions include widespread and locally abundant nodular grains (carbonate and sulphate) and cements (also carbonate and sulphate) that preserve un-compacted and expanded (displaced) grain frameworks. Additionally, some cements have evaporitic textures (e.g. pseudomorphed 'desert rose' forms, enterolithic anhydrite).

The carbonate nodules (calcite and dolomite) are an abundant framework grain constituent throughout the BSF. These are characterised by dominantly rounded sand sized forms with concentric structures defined by sequential zones of micritic and/or radial fibrous carbonate, and

hematitic clays. Nodule cores comprise a mix of silt-grade silicate grains, mixed micrite and clays, and nodule fragments with evidence of varied degrees of reworking. They are most abundant in wells from the central to eastern parts of the study area (Quadrants 43 and 44). These nodules are not ooids *sensu stricto*, because evidence that they formed through *both* surface and shallow sub-surface processes is abundant and widespread.

Carbonate nodules are locally concentrated in laminations and, together with associated eodiagenetic cements, form dolocrete and calcrete layers, mostly hosted in finer grained laminations with sub-millimetre to centimetre (plus) scale thicknesses. Variable lateral continuity typically reflects the structure of the hosting sedimentary laminations. These features present partial barriers to larger scale porosity interconnectivity and are of sub-seismic-resolution.

Subsequent burial diagenesis (mesodiagenesis) is dominated by the formation of further widespread pore-filling cements, mostly of anhydrite and halite. These cements are typically also partially replacive of eodiagenetic nodules. Several episodes of cementation and some of dissolution, have been identified. These are generally poikilotopic cements, which in the case of anhydrite, differentiates it from eodiagenetic sulphate nodules. Anhydrite largely pre-dates halite. Enclosure of anhydrite by halite is largely passive (i.e. anhydrite crystals have euhedral margins), but there is local evidence for dissolution of anhydrite prior to, or during, halite emplacement. Both of these cement phases are preferentially developed in coarser sandstones. Major halite cement is only observed at and below a current burial depth of ~1400 m. This suggests that the halite distribution must be, in part, controlled by current and / or recent conditions. Locally, halite dissolution has occurred preferentially along coarser grained sandstone laminations in otherwise fully cemented intervals.

Diagenetic silicate cements are rare over most of the study area. The exceptions to this are samples from the western edge of the study area (Quadrant 41 wells) where compaction textures are well developed and quartz cement is widespread.

Heterogeneity of compactional textures is a key characteristic of the BSF observed across the study area. On a sub-millimetre scale, areas of well compacted framework grains exist next to areas with open and expanded fabrics. The looser textures can only partially be explained by grain replacement and dissolution, and the current distribution of diagenetic cements. We conclude that the samples were partially cemented prior to maximum burial, but the cement distribution has changed subsequently. It is clear that the halite and anhydrite cements in their current distribution, cannot have been the primary control on the degree of compaction currently observed in the BSF.

This observed textural heterogeneity is consistent with our proposed diagenetic model, which infers that the sandstones had abundant, but not complete, early cements that preserved shallow framework fabrics. As these cements were partial, compactional fabrics were created in the surrounding less- or un-cemented zones. Subsequent dissolution, replacement and / or mobilisation of some or all of the cement phases, post maximum burial, has resulted in the widely recognised heterogeneous compaction fabric which does not correspond to current cement distributions. Since both anhydrite and halite show evidence for both multiple phases of formation and partial dissolution, these are the primary candidate minerals for dissolution / mobilisation. As these phases have also partially replaced some of the framework carbonate nodules, then their subsequent dissolution / mobilisation could also create an apparently uncompacted fabric.

One expected outcome of abundant, pre-maximum-burial cementation, is that BSF porosities should be detached from a simple linear variation with maximum burial depth. This is what is observed for the BSF.

It is recognised that the conclusions of this study are constrained by the limited numbers of samples (for the extent of the study area) and the fact that they are all sourced from hydrocarbon-interest boreholes which have targeted potential reservoir structures. Many of these structures are a consequence of site-specific halokinesis, therefore with potentially atypical thermal, fluid and structural conditions.

Whilst we have gained significant insight into the diagenetic paragenesis, we are unable to adequately predict porosity, a major interest for CO_2 and energy storage interests. This is a consequence of the heterogeneities of the BSF in texture, cement distribution and paragenesis. To improve the remaining knowledge gaps and predictabilities of major reservoir properties, further studies are needed:

1. To obtain a better understanding of the distributions of grain fabrics and diagenetic cements, in order to improve predictability of pore size and connectivity, and porosity distribution at a regional scale:
    - Extend the study to include more samples for detailed modal analysis and minus cement porosity calculation.
    - Apply petrographic image analysis to more samples and a wider range of properties to characterise actual porosity, grain size and compactional fabric distributions.
2. Develop a high-resolution diagenetic sequence through isotopic studies of the main cements, tied to their paragenetic sequencing using:
    - Strontium isotope analysis ($^{87}Sr/^{86}Sr$) to inform the origins of solutes in the diagenetic fluids, and extent of rock-water interaction (target phases - calcite, dolomite, anhydrite and halite).
    - Stable (oxygen, carbon, sulphur) isotope analysis ($\delta^{13}C$, $\delta^{18}O$ and $\delta^{34}S$). These techniques would further inform the mineralisation temperature, and carbon and sulphur sources (target phases - anhydrite, dolomite and calcite cements).
    - U-Pb dating to obtain absolute dates for carbonate mineral formation. Using petrographically-guided targeting, this will place the paragenetic sequence in absolute time. A major issue for this will be potential contamination of the carbonate phases by finely-disseminated hematite, which is known to preferentially concentrate U and Pb.

Acknowledgements

We acknowledge funding from the UK Carbon Capture and Storage Research Centre 2017 (EPSRC Grant EP/P026214/1) and the Industrial Decarbonisation Research and Innovation Centre (EPSRC Grant EP/V027050/1). The research also benefited from British Geological Survey National Capability funding from the Natural Environment Research Council, NERC, including the Permo-Triassic Reservoirs and Storage (PTReS) Project from the Cross-Cutting Projects Theme. Sam Holloway is thanked for initiating early studies of BSF diagenesis.

1 Introduction

The Bunter Sandstone Formation (BSF) in the UK Southern North Sea (UKSNS) is a target for carbon dioxide (CO_2) storage exploration (Oil and Gas Authority, 2021). CO_2 storage in the UK is an important part of the portfolio of technologies that can help the UK achieve net-zero greenhouse gas (GHG) emissions by 2050 (UK Government, 2019).

The BSF is a Triassic age sand sheet complex more than 50 m thick, gently folded into domal periclines (Cameron et al., 1992). A few of these domal structures (commonly referred to as 'closures') contain natural gas and have been extensively studied (e.g. Ritchie and Pratsides, 1993; Bifani, 1986; Ketter, 1991). The saline aquifer parts of the formation have a much larger CO_2 storage potential (The Energy Technologies Institute LLP, 2021) but have very little data available by comparison. The exception is the structure known as 'Closure 35' (Bentham et al., 2006) and more recently as 'Endurance' (Furnival et al., 2014a, b), which was investigated for CO_2 storage via a purpose drilled well in 2010 (Blackbourn and Robertson, 2014). Reservoir properties and facies architecture vary between these more intensively studied locations, but the reasons for existing property distributions are not clear and have been difficult to predict (in the case of Endurance structure). Studies of pressure dissipation in response to CO_2 injection (e.g. Noy et al, 2012; Williams et al., 2014) suggest that any injection into a specific closure would likely affect formation pressures in the surrounding formation. It is therefore important to understand the regional property distribution not just within the closures, for its direct implications on CO_2 injection and containment, but also to understand the potential pressure interaction between any neighbouring sites. Pressure propagation through the reservoir depends on several factors, including flow-path connectivity and tortuosity, together with the porosity and permeability to fluids. It is therefore important to understand the distribution of these properties beyond the more extensively studied, but geographically limited individual structures. Previous studies have highlighted the small scale sedimentary and diagenetic features which can potentially strongly influence fluid flow in the BSF, for example, the occlusion of porosity by halite cements in parts of the reservoir (Bifani, 1986; Ketter, 1991; Ritchie and Pratsides, 1993). Porosity occlusion by halite is particularly problematic to identify on standard geophysical logs, as halite can have a similar signature to natural gas in the pore space. Moreover, water-soluble cements such as halite may or may not be apparent through detailed core examination, depending on the methods of core preservation, the extent of cleaning, and sample cutting and petrographic section preparation methodology used prior to study. Anhydrite, while less readily removed by poor core handling, can also adversely affect log interpretations as its relatively high density could lead to an underestimation of porosity. These factors can limit the ability to understand *in situ* downhole cementation from legacy well data, and its influencing factors remain poorly understood. This study examines 83 samples, 78 of which are from the BSF, across 12 wells in petrographic detail (Figure 1), and adds to the body of research attempting to discern diagenetic histories and their effects on reservoir rock property distributions in the BSF.

1.1 GEOLOGICAL HISTORY OF THE AREA

The UKSNS lies at the western end of the Southern Permian basin which stretches from the east of the UK to the east of Poland (Bachman et al., 2010). It was a depositional centre from the early Permian until the early Jurassic. It is underlain by eroded Carboniferous rocks, which include the hydrocarbon source rocks for the UKSNS. Basin fill began with the aeolian sands and desert lake sediments of the Rotliegend Group, and these now form a major UK hydrocarbon reservoir

(Figure 2). Late Permian sea-level fluctuations coupled with continued basin subsidence, resulted in the deposition of thick, 500 m+ Zechstein carbonate - evaporate cycles that underlie the UKSNS and much of Northern Europe (Johnson et al., 1994). The earliest Triassic saw a return to continental conditions and the deposition of the Bacton Group (the Bunter Shale followed by the BSF) on an extensive flat plain. The Bunter Shale represents distal floodplain and playa-lake clastics that prograded east and northeast from the London-Brabant High. Comprising mostly siltstones and claystones, the unit is more than 300 m thick in the basin centre. Some early sandstones were deposited near the sediment source at the basin margins; these include the Hewett Sandstone which is the major hydrocarbon reservoir for the Hewett gas fields (Johnson et al., 1994).

Sediment for the BSF in the UKSNS was sourced from the London-Brabant Massif and Pennine High to the south and west (Figure 1), and was deposited in the basin under arid to semi-arid conditions, resulting in more than 350 m of sandstones in the Sole Pit Trough (Cameron et al., 1992; Ruffell and Hounslow, 2006). The sheet-flood sand complex is made up of a combination of fluvial channels, coalescing alluvial fans dissected by braided fluvial channels and aeolian dunes with interbedded mudstones deposited in ephemeral lakes (Bifani, 1986). These were draining into a playa lake to the north and north east (Ritchie and Pratsides, 1993). The BSF in the UK is sandier than its eastwards equivalents in Germany and the Netherlands, and so the upward fining cycles seen there are less obvious in the UK, and regional correlation of individual laterally-impersistent clays horizons has been considered impossible (Cameron et al., 1992). However, at a more local scale, the gas field studies have subdivided the formation into 5 to 7 locally correlatable zones, defined by grouping sections of the reservoir by depositional environment or rock properties (Ketter, 1991; Ritchie and Pratsides, 1993). In a regional context, it is likely that some of these subdivisions represent minor hiatuses, unconformities, or changes in sediment transport, as have been identified east of the UK median line. Figure 2 shows the single BSF unit in the UK is equivalent to up to 7 individually correlatable units in the Dutch sector. Geluk (1997) interpreted the latter as having been caused by short lived tectonic uplift relating to the start of the breakup of the Pangea continent, with thermal subsidence prevailing in between, as evidenced by the fairly uniform thickness of the BSF across such a wide area. Two major upwards movements occurred following deposition of the Volpriehausen Formation, with associated periods of erosion. The strongest of these movements was the second uplift event which led to the creation of the widely-correlatable Hardegsen unconformity (referred to as the H-unconformity by Cameron et al., 1992), that separates the BSF from the Haisborough Group rocks in the study area (Figure 2).

During the Mid to Late Triassic, further basin extension triggered the onset of movement of the Zechstein salts (through halokinesis) that underlie the BSF. Structural styles within the UKSNS vary by region, and were controlled largely by underlying basement (pre-Permian) faulting and salt thickness (Underhill, 2009). Within this study's area of interest (Figure 1) the BSF was folded into gentle periclines (domes) and the region became bounded by fault zones and salt-cored anticlines primarily along the Dowsing and North Dogger Fault zones (Figure 1). The growth of these structures controlled subsequent sedimentation and marine incursions. This is reflected in the more variable depositional thicknesses and extent of the late-Triassic Haisborough Group which directly overlies the BSF and Bacton Group and is the primary seal for the BSF hydrocarbon fields. Lacustrine and floodplain conditions with marine incursions resulted in the development of thick carbonate and mudstone accumulations punctuated by evaporite members which are thinner and more locally distributed than the Permian Zechstein evaporites. However, the Haisborough Group is up to 900 m thick in the centre of the Sole Pit Trough (Johnson et al., 1994). Heinemann et al., (2012) examined the total BSF seal thickness and found it generally in excess

of 200 m and in excess of 1000 m in some places. By the late-Triassic and through the Jurassic, there was persistent ocean connection and marine conditions prevailed. Predominantly mudstones and limestones were deposited, although many were subsequently eroded.

Towards the end of the Jurassic through to the Cretaceous, another episode of uplift and erosion occurred, particularly along the Sole Pit Trough (Figure 1). This area was uplifted and inverted to create the Sole Pit High (Japsen, 2000; Bulat & Stoker, 1987 and others) resulting in up to 2 km of erosion in parts of the former trough axis (in Quadrant 48), by the late Cretaceous. This basal Cretaceous (Late Cimmerian) unconformity cuts down through seal rocks into the BSF itself in the eastern half of Quadrant 49 on the Cleaver Bank High. Most of our area of interest is outside of the inversion axis, to the north, but tectonics associated with Sole Pit inversion could have influenced fluid flow and diagenetic events in the Triassic BSF sediments.

During the Cretaceous, with rifting and local inversion continuing, sea level rose, and the Cromer Knoll Group was deposited followed by the extensive Chalk Group. This forms the BSF seal in Quadrant 49 where the Haisborough Group has been eroded, where the seal rocks are reported to be 56 m thick by Heinenman et al., 2012. The maximum burial of the Carboniferous rocks occurred during the Cretaceous, bringing the source rocks to gas maturity (Ritchie and Pratsides, 1993). Gas generation had ceased by the end of the Cretaceous (Grant et al., 2021). It is thought that the salt movement (which started in the Mid to Late Triassic) and associated continuing tectonics enabled pathways for gas to migrate into Triassic BSF while structures were still growing (they are not filled to spill).

Post-Chalk (earliest Palaeogene), further phases of structural inversion and uplift occurred, resulting in erosion and the Base Miocene Unconformity. Halokinesis has continued, spreading across the Sole Pit High area, in the process amplifying folds in the basin centre (Grant et al., 2021).

For most of the sample locations in the study area, it is thought that the maximum burial of sediments occurred immediately prior to a period of Neogene uplift and erosion which exhumed the BSF at the western margins of the Basin (Japsen, 2000). A maximum 1 km of erosion affected the East Midlands Shelf (onshore, where the BSF equivalent Sherwood Sandstone Group is exposed). This reduces to an estimated 0.5 km, out towards the UK-Netherlands median line, parallel to the English coastline (Japsen, 2000).

Further background details on the stratigraphy, structure and petroleum systems of the SNS are described by Cameron et al. (1992) and Underhill (2003).

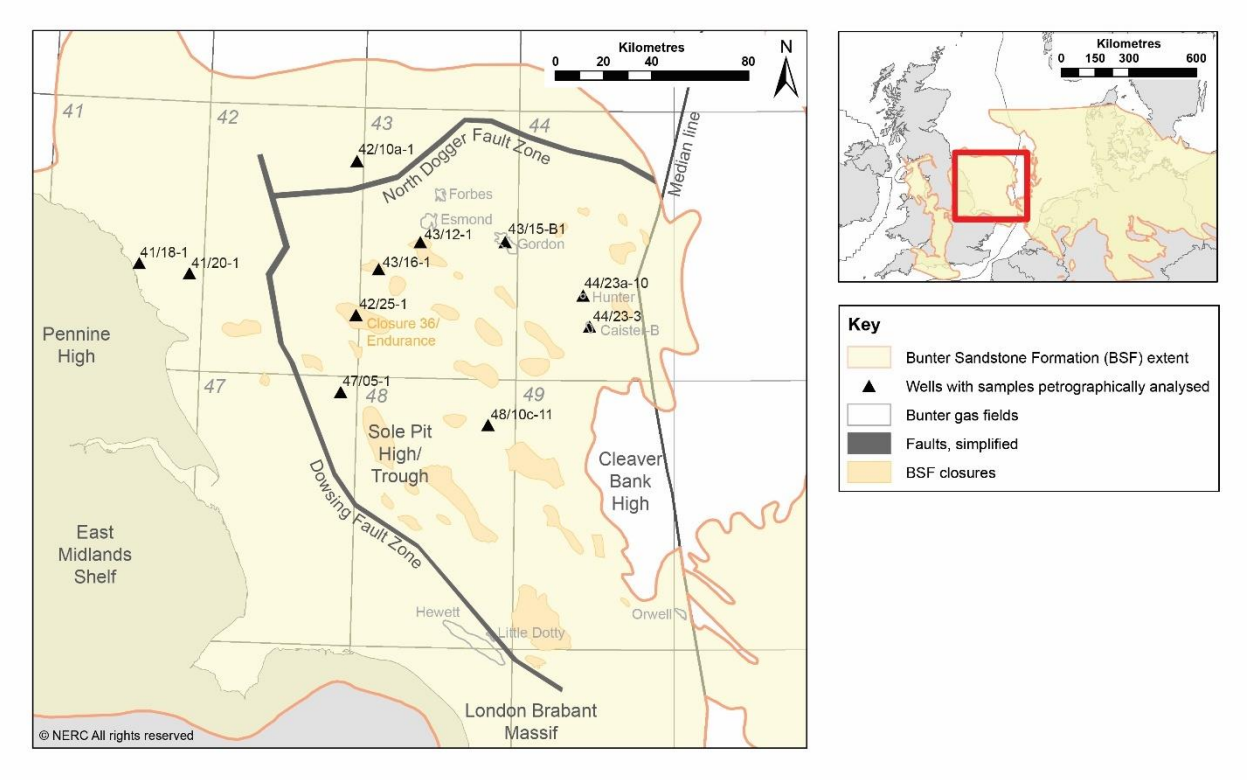

Figure 1 Mapped Bunter Sandstone Formation (BSF) extent in the UKSNS. Petrographic sample distribution shown as black triangles. Key features relating to the topography during the area's geological history are labelled in dark grey text. Offshore quadrant, coastline and field linework contains information provided by the OGA. BSF Closures from the CO2 Storage Evaluation Database (www.co2stored.co.uk). BGS © UKRI.

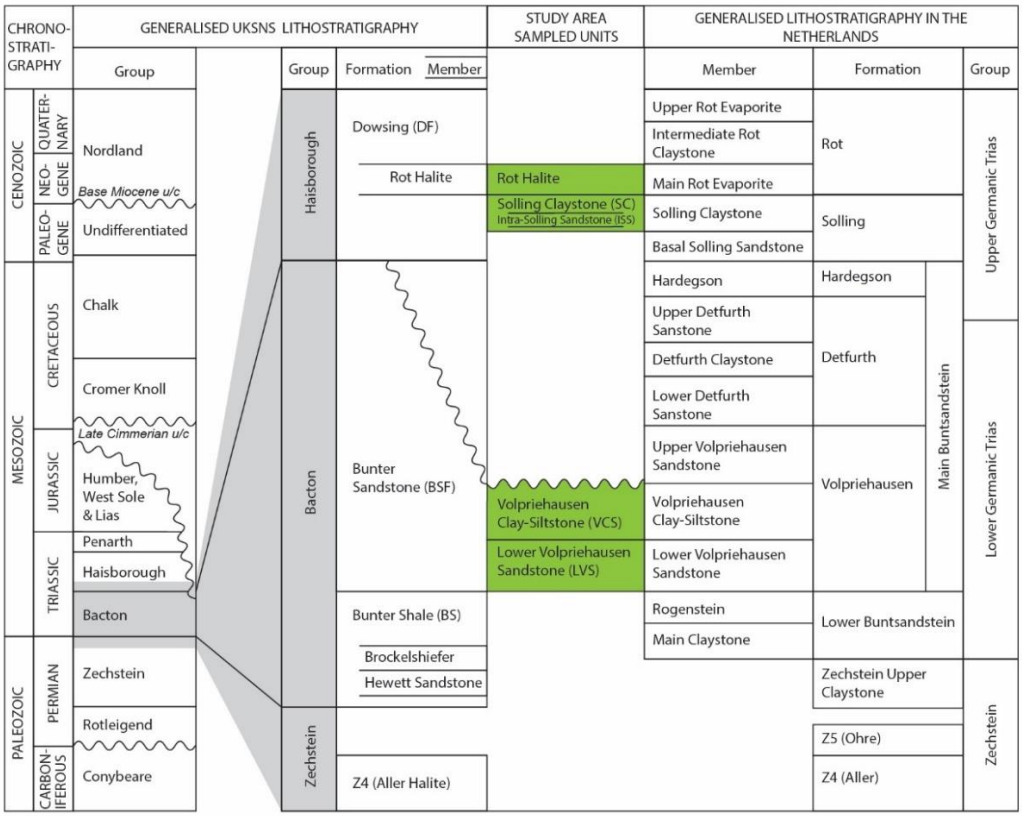

Figure 2 Left: Stratigraphic column showing the relative position of the BSF. Centre-Right: Comparison between the UK and Dutch stratigraphic nomenclature (Johnson et al., 1994; Doornenbal and Stevenson, 2010). The Dutch stratigraphy has been used in this study. The units the petrographic samples are from, and their naming nomenclature are shown in green.

1.2 BUNTER SANDSTONE FORMATION STRATIGRAPHIC ARCHITECTURE

In the Netherlands (and indeed, in all countries where the BSF outcrops to the East of the UK), the BSF is subdivided into several sediment cycles. Geluk (1997) proposed that these were related to climatic cycles caused by the precession, obliquity and eccentricity in the earth's orbit around the sun rather than sea level fluctuations or tectonic events, which were non-uniform across the extensive depositional basin (Figure 2B). These high-resolution cycles are discernible through detailed correlation of wireline logs across the region. The cycles are hierarchical, from the centimetre to decimetre 'low order' fining upwards cycles, to those that occur over several hundreds of metres, 'high order cycles', which are made up of a number of lower order cycles (Geluk, 1997). The sediment cycles are truncated by hiatuses or unconformities throughout relating to episodic uplift and erosion associated with the breakup of Pangea, as mentioned in Section 1. As the BSF is predominantly sandy in the UK, these cycles have proven difficult to differentiate. Nevertheless, for this study, the Dutch nomenclature is used, following from an in-house correlation study (unpublished), which used a combination of different wireline log curves from a multitude of wells across the UKSNS, enabling correlation of the higher order cycles ('Member level') from key Dutch wells across to broadly equivalent units in the UK sector. This allowed the samples from all the wells in this study to be studied relative to their depositional position. The study suggested that the top of the BSF is progressively truncated towards the north in the UK sector, which is perhaps not surprising given that 1–2 km of Mesozoic sediments are thought to have been removed following uplift (Japsen, 2000), particularly along the Sole Pit

trough/high axis (roughly parallel to the Dowsing Fault line) in the UKSNS. The Detfurth and Hardegsen formations are thought to be largely absent from the study area as they have been removed beneath the Hardegsen Unconformity. The samples in this study are therefore considered to be from units broadly equivalent to the Lower Volpriehausen Sandstone (LVS) for the deeper sandier samples, and the Volpriehausen Clay-Siltstone (VCS) for the relatively more clay-rich upper samples. Whilst further work is required to consolidate the regional stratigraphic correlation, the LVS / VCS sub-division employed here provides a convenient means by which to sub-divide the BSF in the study area. It is recognised that using the term Clay-Siltstone for an interval that predominantly comprises sandstone (in the UK sector) is anomalous, however the nomenclature is used here for reasons of lateral correlation. In addition, it became apparent through the correlation study that the Solling Claystone in some areas included an 'Intra-Solling Sandstone' and that in some wells/studies this was interpreted as part of the BSF. Note that the Basal Solling Sandstone in the Dutch nomenclature is indistinguishable on wireline logs in the UK sector, despite being separated by the Hardegsen unconformity and having a different provenance. The Solling units are included within the Dowsing Dolomite Formation, which is part of the Haisborough Group in UK stratigraphy. Gas water contacts were collated from composite logs or interpreted from wireline logs in order to enable consideration of hydrocarbon charge in the interpretation of diagenetic history.

1.3 PREVIOUS BUNTER SANDSTONE FORMATION PETROGRAPHIC STUDIES

Published petrographic studies of BSF diagenesis are few, and compared to the current study they are typically restricted to single fields or geographically constrained areas associated with hydrocarbon industry investigations. All studies from UK and Dutch Sector BSF fields (all are gas fields) have reported the presence of common to abundant diagenetic cements, halite in particular, as well as anhydrite and carbonates. It has been noted previously that the presence of thin, laterally discontinuous halite intervals significantly impedes vertical permeability in the BSF fields (Bifani, 1986). Ritchie and Pratsides (1993), and Poroperm-Geochem (1987) suggested that reservoir porosity occlusion by halite is inhibited in the gas leg. Ketter (1991) mentions that in their reservoir zones 5 and 6, in the lower half of the BSF in the Esmond Field (Block 43/13a), preferential development of abundant diagenetic cementation in the coarser grained sandstones resulted in poorer or more erratic porosity and permeabilities than in the finer grained units. This 'reservoir quality inversion' phenomenon was also reported from the Caister-B field in the UK (Block 44/23a; Poroperm-Geochem, 1987) and from the Netherlands offshore sector (Blocks L and F) by Purvis and Okkerman (1996).

The distribution, timing, and origins of the main cements, particularly the halite, has been a major point of discussion and speculation in these studies. In most cases, halite is described as a late diagenetic cement. For example, Poroperm-Geochem (1987) in a two well study in the Caister-B gas field, suggest that halite was deposited in two episodes, prior to and after gas emplacement. They postulate that the earlier halite was sourced from overlying Triassic evaporites (the same source as the pervasive anhydrite cements) during the late Jurassic Cimmerian uplift and that the later phase came from the underlying Zechstein halokinesis during Alpine structural events in the Miocene. Alternatively, Laier and Nielsen (1989) proposed that halite cementation in an onshore BSF dome structure in Denmark occurred late in its diagenetic history, precipitated from the hyperfiltration of brines forced through shale layers by the emplacement of nitrogen gas into the reservoir.

In contrast to most, Muir *et al.* (1994) concluded from a study of well 49/06a- 4, almost totally cemented by anhydrite and halite (particularly in the upper parts), that these cements formed

concurrently and in the shallow subsurface. They propose that cementation was a consequence of highly saline groundwaters which varied in composition with the climate and paleogeography of the depositional environment of ephemeral streams and lakes. They also described ~3 m scale fining upwards cycles in the core with more calcrete-type carbonate cements in the base and more anhydrite and halite higher up in each cycle. They hypothesise that this vertical variability in cement abundance, and in anhydrite Sr isotope ratios, suggest that the occluding cements were likely not deposited all in one event from late stage vertically migrating brines, as suggested by other authors. The high cement levels are similar to the likely original porosities in ephemeral streams which also suggests the cements were formed prior to significant burial and compaction. The general halite increase vertically through the core could also be due to deposition from the downwards percolation of halite-saturated brines sourced from the later overlying evaporite basin that led to formation of the Röt Halite, again, prior to significant compaction.

The Purvis and Okkerman (1996) study of the offshore Dutch sector L and F blocks included stable carbon, oxygen, sulphur and strontium isotopic analyses of carbonate and sulphate cements. This enabled them to draw conclusions about the sources of the fluids from which these cements precipitated. Using the values obtained for $\partial^{18}O$ (-3.7 to -9.3‰ PDB), $\partial^{13}C$ (-3.0 to +2.9‰ PDB) and $^{86}Sr/^{87}Sr$ (0.7091 to 0.7109) the authors suggest that dolomite cements precipitated from evaporitic meteoric pore waters in near surface conditions with sparse organic-matter, a finding that is consistent with the proposed semi-arid to arid continental depositional model. The majority of the anhydrite cement isotopic values ($\partial^{34}S$ +4.2 to +12.1‰ CDT) matched those of the Zechstein evaporites (except in part of one well where it matched oxidation of sulphide-containing source rocks), rather than the overlying Haisborough Group that Poroperm-Geochem (1987) had suggested as the mostly likely source in Caister-B. In the absence of evidence for gypcrete in their study area, they concluded that the Zechstein was the most likely source for the early anhydrite as well as for the halite. In contrast to other studies, Purvis and Okkerman (1996) inferred that these were early cements because in many samples they infill pores with no other cements. They theorised that saline brines arising from the transformation of gypsum to anhydrite in the underlying Zechstein, were introduced into the BSF through hydrofracturing of the Bunter Shale. Flow of these brines, as well as any ground waters, was concentrated along those beds with the best porosity and permeability characteristics, hence the concentration of anhydrite and halite in them. Halite cement was not associated with shale baffles in their study area, so they thought the hyperfiltration emplacement mechanism proposed by Laier and Nielsen (1989) in their Danish study area was unlikely.

Spain and Conrad (1997) studied seal rocks and one reservoir core from a Netherlands offshore well (P block), and did not report any halite cementation. They reported frequent, irregular diagenetic cementation contacts, cross-cutting bedding in the upper part of the reservoir, and suggested these contacts could represent palaeo-groundwater tables. Overall, the main cements present were dolomite with some anhydrite, and the degree of intergranular cementation strongly controlled the reservoir quality. Local dissolution of the anhydrite had created the best reservoir quality and the degree of cementation was interpreted to be controlled by “i) the emplacement of early anhydrite cement which prevented severe compaction; ii) detrital illitic grain-coating clays which inhibited subsequent quartz and feldspar overgrowths; iii) pore-filling and replacement by pyrite, dolomite, and siderite cement; iv) dissolution of feldspar grains in poorly cemented sandstone; and v) the dissolution of anhydrite cement and replacement anhydrite”.

Van Bergen and De Leeuw (2001) modelled halite plugging mechanisms of overpressured BSF reservoirs in the Netherlands blocks L2 and F15. In L2 this was observed 1.5 km from the diapir. Previous interpretations of salt plugging in these reservoirs involved seepage from overlying

evaporites, an early diagenetic process. However, they suggest that the plugging occurred later in the diagenetic paragenesis, as a result of the temperature gradient distortion that occurs around salt domes (as they have a higher thermal conductivity than the surrounding siliciclastics). The retreat of Zechstein salt strata from the sedimentary sequence between diapirs allowed the vertical migration of overpressured, saturated Permian brines. The brines migrated laterally once in the BSF, and halite was precipitated when it reached the relatively lower temperature strata adjacent to the salt domes. Concentration precipitation mechanisms were considered, but discounted as less likely, because higher density brine flowing upgradient is unlikely and a low permeability overburden would inhibit the necessary mixing. In addition, the brine influx – temperature distortion model accounts for all the halite, whereas there is a mass balance deficit if only the formations above the main Zechstein evaporites are considered.

Dingwall et al. (2013) discuss a seismic polarity reversal observed on seismic reflection data around the domal structure straddling UKSNS Quadrants 42 and 43 (known as 'Endurance'), a structure licenced for CO_2 storage. They interpreted it as the transition between good and poorer quality reservoir rock, based on petrophysical logs either side of it. The polarity reversal marks a cemented 'hard ground', with calcite and halite cements occupying the pore space beneath (and outside of) the phase reversal. Proposed mechanisms explored by 1D modelling were that meteoric influx via a BSF seabed outcrop occurred when it was likely subaerially-exposed during and after the last ice age. The less saline and more buoyant meteoric fluids would have primarily affected the upper reservoir by either diluting the *in situ* brines to a concentration below halite saturation, or by dissolving out existing halite cements, and resulting in the generation of secondary porosity. Note that this study was carried out prior to the drilling of well 42/25d- 3 and brine samples being available, which helped to offer an alternative scenario more similar to that of Van Bergen and De Leeuw (2001).

Blackbourn and Robertson (2014) conducted a detailed sedimentological and petrographic study of the diagenesis and burial history in the offshore UK well 42/25d- 3 drilled into the Endurance structure for CO_2 storage appraisal (Figure 1). Major cements were dolomite and anhydrite, formed early in burial diagenesis and notably, very little halite. They propose that halite had initially been present patchily, as found in other wells regionally, but that it had been removed via thermohaline convection cells exchanging fluids where they adjoined, together with limited meteoric influx from the seabed outcrop at the crest of a salt diapir to the East. This exposure may have occurred since either the late Jurassic uplift or during the early Tertiary uplift. Compared to global porosity versus depth relationships (with appropriate caution) the BSF has a 7% higher porosity than expected. This could have been created primarily by late-stage halite dissolution, as of the dissolution of other cements volumetrically do not appear to account for this abnormally high porosity.

Blackbourn and Robertson (2014) note the presence of a several-feet-thick calcareous interval in the crestal well of the structure (42/25- 1), which contains what they identified as reworked Bunter Shale ooids, and which could act as a vertical permeability baffle (one sample was 65% by volume carbonate, and had a permeability of 44 mD). 1D burial modelling suggested the maximum burial of ~2500 m occurred during the Late Cretaceous, but that maximum temperatures of 115-130°C occurred during Late Jurassic and Early Tertiary episodes.

These studies generally agree that the porosity and permeability of the BSF are controlled both by the original depositional texture and by subsequent diagenesis. Timings and mechanisms have been proposed from one UK field (Poroperm-Geochem, 1987), and study areas in neighbouring countries (Laier and Nielsen, 1989; Purvis and Okkerman, 1996). However, a more regional

understanding of the diagenetic history and current reservoir quality has not been published for the UK. This is therefore the aim of this study.

2 Sampling

New samples were taken from a wide range of legacy hydrocarbon industry borehole materials stored at the National Geological Repository, with a total of 83 samples from the BSF taken from 12 wells across the UKSNS (Figure 1, Table 1). Note that 47/05- 1 samples were from cuttings, while all others were from drill core. The samples examined were from a number of different BGS projects with differing objectives, and do not represent an exhaustive nor fully representative set for the BSF across the UKSNS. The observations and deductions reported below must be taken in this context; as Table 1 shows, sampling is biased stratigraphically to the middle of the VCS and the top of the LVS members, and geographically to Quadrant 44 wells. The bias comes from the preferential targeting of these units by the hydrocarbon industry as the primary targets for gas.

Summary details of the samples analysed are given in Table 2.

Table 1: Distribution of samples by location and equivalent stratigraphy.

Well	**No. of samples**	**Stratigraphy***						
		DF / ISS / SC	Bunter Sandstone Formation					
			top VCS	mid VCS	base VCS	top LVS	mid LVS	base LVS
41/18- 1	**2**	-	-	2	-	-	-	-
41/20- 1	**2**	-	-	2	-	-	-	-
42/10a- 1	**4**	2	-	-	-	-	-	2
42/25- 1	**4**	-	4	-	-	-	-	-
42/25d- 3	**10**		10	-	-	-	-	-
43/12- 1	**5**	-	-	2	-	3	-	-
43/15-B1	**4**	2	-	2	-	-	-	-
43/16- 1	**3**	-	-	3	-	-	-	-
44/23- 3	**19**	1	-	12	3	3	-	-
44/23a- 10	**15**	-	-	9	2	4	-	-
47/05- 1[#]	**3**	-		1			2	
48/10c- 11	**12**	-	-	4	1	3	4	-
Total	**83**	**5**	**4**	**37**	**6**	**13**	**6**	**2**

* Key: DF – Dowsing Formation ISS – Intra-Solling Sandstone
SC – Solling Claystone VCS – Volpriehausen Clay-Siltstone
LVS – Lower Volpriehausen Sandstone

[#] - Samples from cuttings.

3 Methods

The samples were impregnated with blue-dyed resin and prepared as polished thin sections (PTS) to a standard thickness of 30 µm. They were examined using a combination of optical petrographic microscopy, high-resolution backscattered electron (BSE) imaging scanning electron microscopy (SEM) with mineral identification aided by qualitative energy-dispersive X-ray (EDX) microanalysis, optical cold-cathodoluminescence (CL) microscopy, and SEM cathodoluminescence imaging (SEM-CL). Selected samples were also prepared as rough stub mounts and examined by secondary electron (SE) imaging in the SEM.

A selection of sections was additionally analysed by automated quantitative mineralogy (AQM) using Zeiss Mineralogic phase-mapping software (V1.6.2) hosted on a Zeiss Sigma 300 field emission scanning electron microscope (SEM), fitted with twin Bruker Xflash 6|30, 30 mm^2, 129 eV resolution, energy dispersive X-ray (EDX) detectors. AQM phase maps were generated with the SEM operating at 20 kV, 10 mm working distance, with a 120 µm aperture and 'beam boost' activated to give a nominal beam current of 10 nA. Mapping was performed over a grid of frames controlled by Mineralogic automated mosaicking protocols. BSE images and EDX data were captured in turn for each frame, with a beam step size of 10 µm and a dwell time of 20 ms for gathering the EDX data. BSE images were captured with a 0.1 ms dwell time at a range of resolutions to match the scale of textural features, typically with a beam step size of 5-10 µm. Phase identifications were based on the per-pixel-normalised quantitative EDX data (using ZAF quantification protocols) passed through expert-user-defined compositional filters. Data outputs comprise mosaicked phase map and BSE images, and quantitative modal mineralogies. For this group of samples (excepting those from 42/25d- 3), quantitative porosity was determined using petrographic image analysis (PIA) applied to the mosaicked BSE images. The PIA was performed using ImageJ (v2) software, binarising the images to separate porosity by thresholding to low brightness (the resin used to impregnate the porosity is black or near black under the BSE imaging conditions used), and the 'region of interest tool' to select areas of the images unaffected by artefacts (e.g. sampling-induced fractures). The AQM and PIA results are presented in Table 3.

Minus-cement porosity (a term introduced by Rosenfeld, 1949) is widely used in sedimentary petrography. It is obtained by adding the area of diagenetic cements occupying primary (inter-granular) porosity (corrected from modal to whole-volume values) to the residual primary porosity. It is particularly used to inform the roles of compaction and diagenetic cementation in porosity evolution, specifically with respect to the relative timing of cementation events against burial. There are inherent complications in the application of this approach (the role of matrix, ductile grains, degree of chemical compaction; summarised by Paxton et al., 2002), but it can provide a useful picture of the compactional state of the aggregate when diagenetic cement(s) formed. This value was calculated for those samples with both AQM-derived mineralogies and PIA-derived porosities. Where necessary, secondary porosity and grain-replacive cement volumes were additionally derived by point-counting using a combination of BSE, phase map and in some cases, CL images.

Table 2: Sample list and analyses performed.

Well	NGR sample No.	MPL code	Depth (m)	SEM	Optical microscopy	Cathodo-luminescence	AQM	Stratigraphy*	Gas / Water leg
41/18- 1	SSK16097	MPLT047	511.00	X	X		X	mid VCS	W
	SSK16096	MPLT046	520.14	X	X			mid VCS	W
41/20- 1		MPLK651	447.90	X	X			mid VCS	W
		MPLK652	448.13	X	X			mid VCS	W
42/10a- 1		MPLK653	1118.75	X	X			DF	W
		MPLK654	1137.35		X			DF	W
		MPLK655	1259.50		X			base LVS	W
		MPLK656	1269.70		X			base LVS	W
42/25- 1		MPLK657	1134.40	X	X			top VCS	W
	SSK7150	MPLT042	1137.30	X	X		X	top VCS	W
	SSK7151	MPLT043	1142.48	X	X	X	X	top VCS	W
	SSK7152	MPLT044	1145.50		X			top VCS	W
42/25d- 3	SSK136727		1431.90		X		X	top VCS	W
	SSK136728		1434.99	X	X		X	top VCS	W
	SSK136384		1436.19	X	X		X	top VCS	W
	SSK136921		1440.08		X		X	top VCS	W
	SSK136922		1444.71		X		X	top VCS	W
	SSK136923		1449.63		X		X	top VCS	W
	SSK136927		1451.43	X	X		X	top VCS	W
	SSK136928		1452.23	X	X		X	top VCS	W
	SSK136924		1453.29		X		X	top VCS	W
	SSK136925		1457.43	X	X		X	top VCS	W
43/12- 1	SSK16098	MPLT048	1388.52	X	X		X	mid VCS	W
	SSK16099	MPLT049	1391.87	X	X		X	mid VCS	W
	SSK16100	MPLT050	1426.46	X	X			top LVS	W
	SSK16101	MPLT051	1428.75	X	X	X	X	top LVS	W
	SSK16102	MPLT052	1430.27		X			top LVS	W
43/15-B1		MPLK658	1639.52		X			ISS	G
		MPLK659	1650.34		X			SC	G
		MPLK660	1658.11	X	X			mid VCS	G
		MPLK661	1670.91	X	X			mid VCS	G
43/16- 1		MPLK662	933.07	X	X			mid VCS	W
		MPLK663	937.41	X	X			mid VCS	W
		MPLK664	945.57	X	X			mid VCS	W
44/23- 3		MPLK665	1362.91	X	X			SC	G
		MPLK666	1364.28	X	X			mid VCS	G
		MPLK667	1371.45		X			mid VCS	G
	SSK7137	MPLT037	1374.80	X	X	X	X	mid VCS	G
		MPLK668	1379.52		X			mid VCS	G
		MPLK669	1380.44		X			mid VCS	G
		MPLK670	1391.56		X			mid VCS	G
		MPLK671	1393.67		X			mid VCS	G
		MPLK672	1398.19	X	X			mid VCS	G
		MPLK673	1401.52		X			mid VCS	G
		MPLK674	1405.43	X	X			mid VCS	G

Well	NGR sample No.	MPL code	Depth (m)	SEM	Optical microscopy	Cathodo-luminescence	AQM	Stratigraphy*	Gas / Water leg
	SSK7138	MPLT038	1414.58	X	X			mid VCS	G
		MPLK675	1415.87	X	X			mid VCS	G
	SSK7139	MPLT039	1421.89	X	X			base VCS	G
		MPLK676	1427.02	X	X			base VCS	G
	SSK7148	MPLT040	1431.04	X	X		X	base VCS	G
		MPLK677	1441.32	X	X			top LVS	W
	SSK7149	MPLT041	1442.47	X	X		X	top LVS	W
		MPLK678	1448.10	X	X			top LVS	W
44/23a-10	SSK7140	MPLT022	1847.75		X			mid VCS	G
	SSK7141	MPLT023	1849.75		X			mid VCS	G
	SSK7142	MPLT024	1855.30	X	X		X	mid VCS	G
	SSK7143	MPLT025	1861.25		X			mid VCS	G
	SSK7144	MPLT026	1870.35		X			mid VCS	G
	SSK7145	MPLT027	1878.25		X			mid VCS	G
	SSK7146	MPLT028	1891.40		X	X		mid VCS	G
	SSK7147	MPLT029	1898.75		X			mid VCS	W
	SSK7130	MPLT030	1903.75		X			mid VCS	W
	SSK7131	MPLT031	1907.25		X			base VCS	W
	SSK7132	MPLT032	1912.00	X	X			base VCS	W
	SSK7133	MPLT033	1918.10		X	X		top LVS	W
	SSK7134	MPLT034	1918.23	X	X		X	top LVS	W
	SSK7135	MPLT035	1921.60	X	X	X	X	top LVS	W
	SSK7136	MPLT036	1924.05		X			top LVS	W
47/05- 1#	SSK16104	MPLT068	1060.70		X			mid VCS	W
	SSK16105	MPLT069	1121.66		X			mid LVS	W
	SSK16106	MPLT070	1176.53		X			mid LVS	W
48/10c-11	SSK16115	MPLT060	2001.32	X	X			mid VCS	W
	SSK16116	MPLT061	2016.56	X		X	X	mid VCS	W
	SSK16117	MPLT062	2033.02		X			mid VCS	W
	SSK16108	MPLT053	2050.08		X			mid VCS	W
	SSK16109	MPLT054	2068.07		X			base VCS	W
	SSK16110	MPLT055	2080.87	X	X		X	top LVS	W
	SSK16118	MPLT063	2085.75		X			top LVS	W
	SSK16111	MPLT056	2100.68	X	X	X	X	top LVS	W
	SSK16113	MPLT058	2112.57	X	X			mid LVS	W
	SSK16126	MPLT064	2121.71		X			mid LVS	W
	SSK16114	MPLT059	2123.54		X			mid LVS	W
	SSK16112	MPLT057	2130.86	X	X			mid LVS	W

* Key: DF – Dowsing Formation ISS – Intra-Solling Sandstone
SC – Solling Claystone VCS – Volpriehausen Clay-Siltstone
LVS – Lower Volpriehausen Sandstone

- Samples from cuttings.

4 Results

4.1 DEPOSITIONAL CHARACTERISTICS

4.1.1 Sandstones

The BSF samples examined vary between quartz arenites, subfeldspathic arenites and sublithic arenites (classification according to Pettijohn et al., 1987, and based on selected modal analysis and visual estimation). They are composed of major detrital quartz with subordinate to minor feldspar (K-feldspar and plagioclase (mostly albite), with rare perthite), lithic clasts (including: chert grains, siltstone, mudstone, lesser quartz-feldspathic rock fragments, and rare altered volcanic fragments). There is a stratigraphic control on the relative abundancies of K-feldspar and albite, with the latter typically the most abundant feldspar in the VCS (particularly in the middle to upper parts). Conversely, K-feldspar is the dominant feldspar type in the LVS.

The sandstones are commonly laminated with parallel and low-angle cross-bedded lamination, and ripple lamination is locally evident (Figure 3A,B). The lamination is mostly defined by coarser and finer sand and silt laminae and alignment of elongate grains. Some beds of sandstones show upwards-fining textures; varying from coarse sandstone at the base, to medium, fine and very fine sandstone and siltstone towards the top. Overall, most sandstones are very fine- to medium-grained, with some horizons of medium- to coarse-grained sandstone and siltstone. There are occasional interbedded mudstone and muddy laminae, and penecontemporaneous rip-up clasts of ductile red mudstone (Figure 3C,D). The widespread fabric of clays in-filling hollows in sand grain surfaces (Figure 4A), shows that many grains were deposited with inherited clay coatings (Wilson, 1992). Generally, the sandstones of the LVS, particularly near its top where medium- and coarse-grained intervals are common, are coarser grained than are those of the VCS, which are mostly fine to very fine grained.

In most of the sandstones, the detrital grains are predominantly angular or sub-angular to sub-rounded with well-rounded grains being relatively uncommon and represented mostly within the coarser sand fraction. However, the sandstones from the top of the LVS, and from the base and middle of the VCS in wells 44/23- 3 and 44/23a- 10 (Figure 14D, Appendix X1) are dominated by fine- to coarse-sandstones with well-rounded sand grains. Similar but less significant increases in rounded grain content were also noted in wells 43/15-B1 and 48/10c- 11.

This observed higher abundance of well-rounded grains is taken as an indication of an increased input of aeolian sand or reworked aeolian sandy sediment during the middle period of BSF deposition, in the central area of the basin (Figure 1), which corresponds to the eastern part of the present study area.

4.1.2 Mudstones and Siltstones

Anhydritic and dolomitic mudstones and siltstones occur interbedded within the sandstones of the BSF (VCS) sequence, and within the overlying Dowsing Formation (Intra-Solling Sandstone and Solling Claystone Members). The mudstones are characteristically red but commonly contain green grey (‘bleached’) bands and reduction spots. They vary from massive silty mudstone to finely laminated mudstone, with thin siltstone and very fine sandstone laminae and interbeds (Figure 3E). Desiccation cracks infilled with siltstone to fine sandstone are locally present, and there is minor evidence of possible bioturbation. These rocks commonly contain disseminated dolomite, and their depositional fabric is commonly disrupted by displacive early authigenic nodules of dolomite and enterolithic nodular anhydrite (Figure 3F).

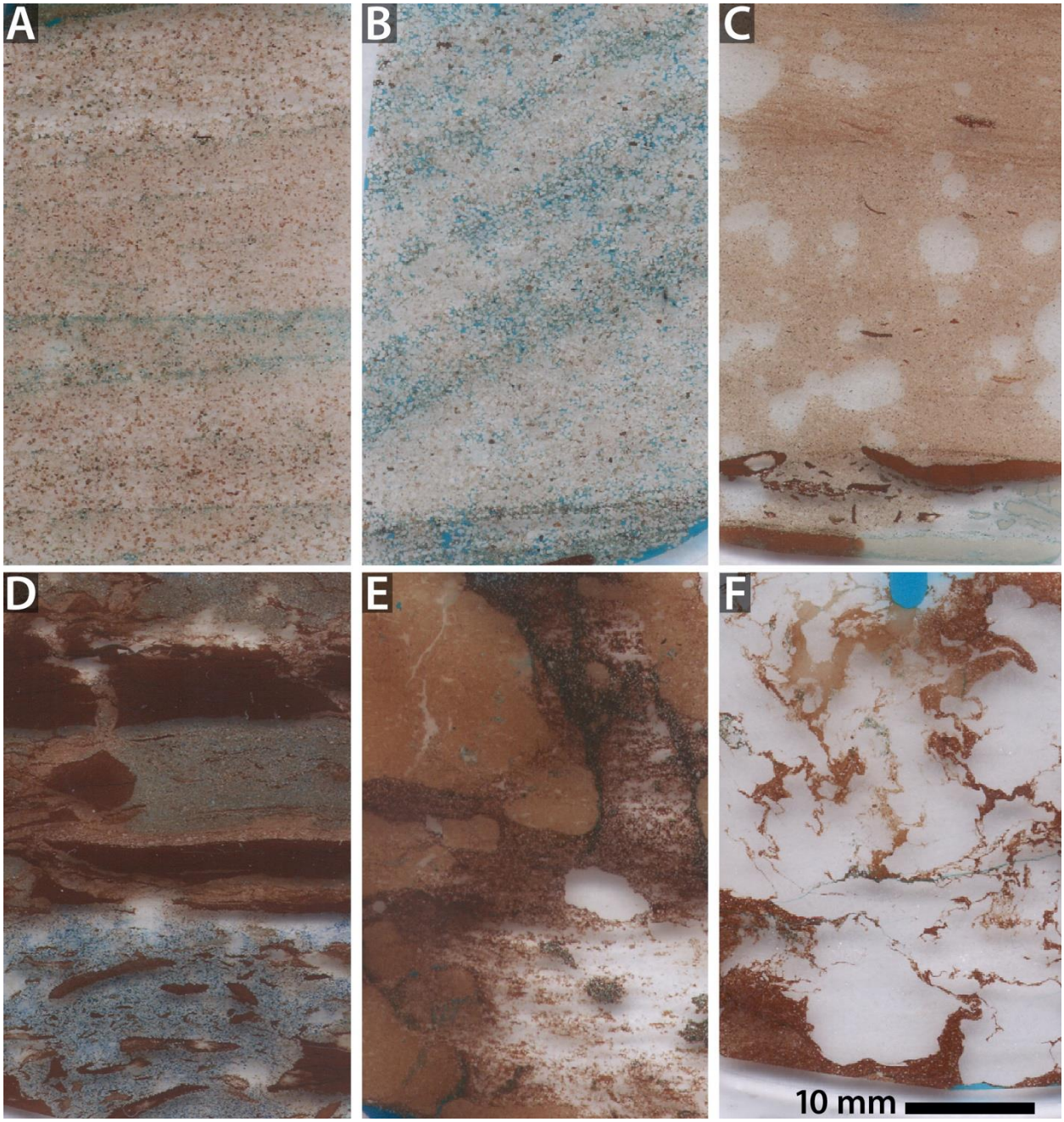

Figure 3: Highlighting depositional textures.
Full thin sections in transmitted light: blue dye highlights porosity, scale bar applies to all. (A) Parallel-laminated very fine sandstone and siltstone, almost fully cemented by poikilotopic halite (mid VCS, 43/15-B1, 1658.1 m); (B) Cross-bedded lamination in fine to medium sandstone; anhydrite preferentially cements some laminae (mid VCS, 41/20- 1, 448.1 m); (C) Ripple-laminated very fine sandstone and siltstone, with intraclasts and thin laminae of red mudstone, and bleached patches cemented by nodular anhydrite (Bunter Shale Formation, 42/10a- 1, 1269.7 m); (D) Thinly-interbedded mudstone, siltstone, and sandstone with mudstone intraclasts. Sub-vertical fractures in the mudstone are filled by silt probably injected during dewatering (mid VCS, 44/23- 3, 1393.7 m); (E) Ferruginous, red siltstone and mudstone, disrupted and pseudo-brecciated (by dewatering and / or collapse after the dissolution of evaporite cements), with early displacive dolomite nodules. (mid VCS, 44/23- 3, 1371.45 m); (F) Red silty mudstone with enterolithic and nodular eodiagenetic anhydrite (mid VCS, 44/23- 3, 1364.3 m).

4.2 DIAGENESIS

The BSF has been subject to significant diagenetic alteration, which has modified both the mineralogy and the porosity (and also by inference, the permeability) of the sandstone reservoir rocks. This has involved both loss of porosity through compaction and cementation, and rejuvenation and enhancement of porosity through de-cementation and framework grain (detrital grain) dissolution. The diagenetic evolution can be subdivided, based on the classification of Schmidt and McDonald (1979a), according to whether the diagenesis is related to: processes occurring in the near-surface (syn-sedimentary) environment prior to significant burial (eodiagenesis); processes occurring during burial and compaction (mesodiagenesis); and near-surface processes affecting the rocks after uplift (telodiagenesis).

Although the aquifer properties of the BSF on the onshore western platform of the basin are markedly influenced by meteoric invasion and associated telodiagenetic alteration (Bath et al., 1986; Monaghan et al., 2012), telodiagenetic alteration is not evident within most of the deeper basin area in the east. However, as noted above, parts of the basin have been subjected to periods of uplift, locally to the near surface as a result of halokinesis. Therefore, this cannot be ruled out as a localised process, and the higher secondary porosity noted in samples from well 42/25- 1 may be a consequence of telodiagenesis.

4.2.1 Eodiagenesis

4.2.1.1 INFILTRATED CLAY AND IRON OXIDE

The BSF exhibits a wide variety of fabrics interpreted to be eodiagenetic in origin. Fine dirt fringes and veneers or “pellicles” of red, ferruginous (hematitic) detrital clay coating the surfaces of detrital sand grains are ubiquitous in the sandstone (Figure 4A, B). These comprise predominantly illitic clays with grain-tangential fabrics, in which the hematitic content is implicit from their colour, but is rarely resolvable as a distinct phase.

The clays have patchy distributions and varied thicknesses, locally bridging between grains, and are also present at some grain contact sites, including sites showing significant compaction. Locally, the clay is concentrated on the underside of the coarser sand grains creating a “bearded” grain fabric. These are all characteristics consistent with the deposition of suspended clay sediment that infiltrated through the sand in the near-surface. These infiltrated clays can be readily distinguished from the inherited clay grain coatings (Wilson, 1992) which underlie the infiltrated clays and are generally more densely packed and darkly pigmented (Figure 4A).

The very early origin of these clays is supported by their observed occlusion beneath other cements, including authigenic quartz and feldspar overgrowths, and pore-filling halite, calcite, and anhydrite (Figure 4). The exception is in rare instances of patches currently cemented by anhydrite, where infiltrated clays are absent; this is evidence that these occurrences of anhydrite, or a pre-cursor phase, formed before any significant infiltration of detrital clay.

Detrital iron and titanium oxides (e.g. magnetite, ilmenite), and other ferromagnesian minerals initially present in these coatings have broken down and are partially replaced by microcrystalline hematite and anatase, and the iron released from the alteration of these minerals probably provided much of the iron for the disseminated hematite that formed within the infiltrated clay films. Such oxidative alteration of detrital ferromagnesian minerals and iron-titanium oxides, and the development of hematic infiltrated clay coatings, are characteristic of eodiagenetic ‘red-bed’ weathering seen in modern sediments in hot arid or semi-arid environments (e.g. Walker *et al.*, 1978), and these fabrics have been reported from the BSF by previous authors (Purvis and

Okkerman, 1996; described as ‘detrital hematite’; Muir et al., 1994; described as diagenetic hematite) and are commonly observed elsewhere in -equivalent red-bed sequences onshore in the U.K. (Sherwood Sandstone Group, e.g. Burley, 1984; Knox et al.,1984; Strong and Milodowski, 1987; Strong et al., 1994; Milodowski et al., 1998; Plant et al., 1999; Monaghan et al., 2012).

Biotite and other micas also display exfoliation with expanded cleavage laminae (Figure 4B, Figure 6A) locally impregnated with fine grained secondary hematite and titanium oxide. This is likely related to vermiculitization of the mica within the near-surface sediment or soil zone (c.f. Burley, 1984).

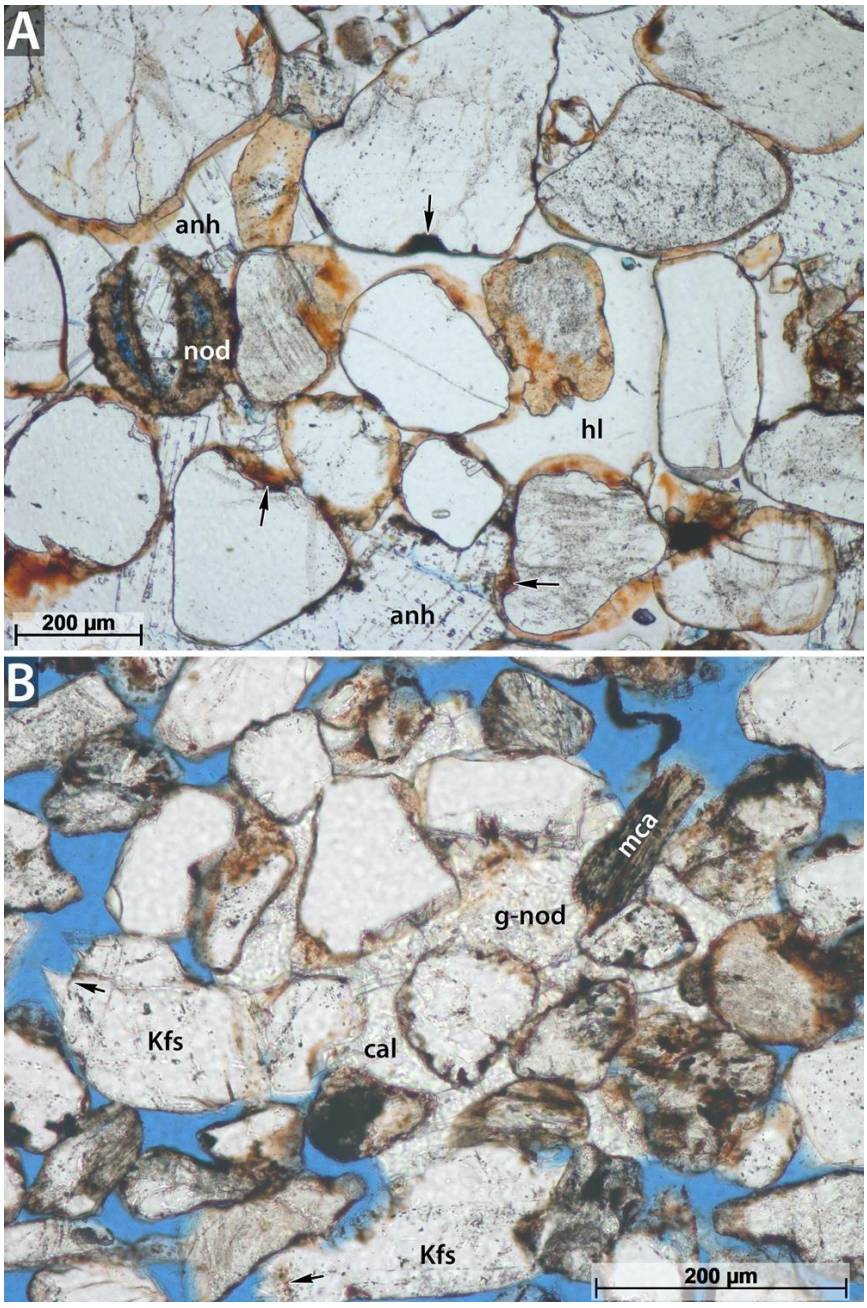

Figure 4: Examples of grain-coating clay forms, cement relationships and textures. Optical PPL. (A) Well-developed red-coloured hematitic grain-coatings with the asymmetric (geopetal) thickness typical of infiltrated origins, enclosed by halite (hl) and anhydrite (anh) cements. Denser fills in grain surface hollows (arrowed) indicate inherited (detrital) origins. Note the calcite nodule (nod) with an anhydrite fill (mid VCS, 44/23a- 10, 1861.3 m). (B) Patchy infiltrated red-brown grain-coatings are cemented by calcite (cal) which has also enclosed an expanded hematitised

mica (mca). Within the calcite is a remnant hematitic clay rim defining a 'ghost' carbonate nodule (g-nod). Minor K-feldspar (Kfs) overgrowths have formed over the clay coatings (arrowed). (top LVS, 48/10c- 11, 2085.8 m).

4.2.1.2 EARLY CARBONATE CEMENTS

Evidence for early carbonate formation was observed in many of the samples examined from all the wells studied across the study area. Much of this is in the form of grain-like carbonate 'nodules' (characterised in Figure 5 through to Figure 8). These are most abundant in wells from the central to eastern parts of the study area (43/12- 1, 43/15-B1, 43/16- 1 and 44/23- 3; Figure 1). They include both calcite and dolomite nodules, which share features that indicate similar origins. They are characterised by sand-sized spheroidal nodules containing multiple bands of hematitic clay inclusions (Figure 5, Figure 6, Figure 7) nucleated around a core that is mostly formed of muddy and silty micrite (Figure 6). They typically occupy framework grain positions in the sandstones (Figure 5, Figure 6, Figure 8), but also have associated textures that suggest displacive *in situ* shallow subsurface growth, whilst some also show evidence for local reworking. Carbonate nodules are dispersed throughout the BSF interval, but are also present in local concentrations where silicate grains are virtually excluded, forming discrete millimetre-scale calcrete and dolocrete laminae (Figure 5). Calcrete and dolocrete laminations are commonly, but not exclusively, preferentially developed in finer grained layers.

Calcite nodules

These comprise rounded grains of neomorphic near-equigranular subidiotopic to xenotopic microspar, or micritic calcite (Figure 6), characteristically with cores and concentric to eccentric bands enriched in hematitic clays. They have varied shapes, mostly rounded to subrounded, and are rarely spheroidal. They are both CL-luminescent manganoan and non-luminescent non-ferroan, non-manganoan (Figure 5). They occur as scattered, isolated sand-sized nodules, or in local concentrations of similarly sized nodules. They locally form an abundant component of calcrete horizons (Figure 5, Figure 6C) where they are cemented by eodiagenetic calcite cement. With their common associated fringing cement (see section below), they commonly support and preserve an open uncompacted detrital grain framework (Figure 5, Figure 6). Optical and BSE microscopy show that the nodules often have a fabric of stellate or radial fibrous to epitaxial calcite (cf. Bathurst, 1975, p.484) commonly seeded upon microporous 'dirty' micritic cores (Figure 6E, F) locally including silicate silt grains (Figure 6I), or small micritic intraclasts (Figure 5, Figure 6D). Some carbonate nodules are also present as variably abraded angular fragments, and concentrated as detrital grains along specific laminations in the sandstone, indicating that some have been through a process of reworking. Rare nodules contain fragments of other nodules as their cores (Figure 6H), providing further evidence of penecontemporaneous erosion and reworking. The bands of hematitic clays typically have varied and uneven (Figure 6D) separations and thicknesses. Notably, nodule-like internal fabrics were observed in rare meniscal and droplet-like patches hosted on silicate framework grains (new Plate).

A range of textural fabrics have been recognised in the sandstones associated with these carbonate nodules. In some parts, the surrounding detrital grains have a 'floating' or expanded grain fabric (Figure 6A, D, F). It is also common, however, for the nodules to partially enclose adjacent framework grains, with the latter cross-cutting some of the internal concentric layered structures of the former with (Figure 6D) and without (Figure 6F, I) evidence for compactional deformation.

Other early calcite cements

Weakly ferromanganoan calcite cement often occurs as later fringing cements nucleated on the calcrete nodules (Figure 5, Figure 6). It typically displays euhedral terminations into open pore spaces with multiple internal growth zones (Figure 5) and can be enclosed by diagenetic anhydrite and halite (Figure 6D) cements. The ferromanganoan composition of the calcite is consistent with it having formed in a deeper groundwater environment than the earlier, nodular calcite, where conditions were sufficiently reducing to form Fe^{2+} and Mn^{2+} species. This generation of calcite can be seen locally to displace grain fabrics and cement weakly-compacted sand grains, consistent with formation prior to significant burial and overburden. This is supported by evidence of compactional deformation textures related to the presence of nodule-fringing cements, which must have occurred after their growth (Figure 6E). However, there are also fringing cements with similar chemical and morphological characteristics that do not show the displacive characteristics, suggesting their formation extended from eodiagenesis into early mesodiagenesis.

Early dolomite cements

Dolomite is a major early diagenetic cement in both mudstone and sandstone-siltstone lithologies, and occurs widely throughout the basin (Appendix X1). Additionally, in some sandstones (Wells 43/15-B1, 43/16- 1, 44/23- 3), dolomite occurs as nodules similar to the calcite nodules described above (Figure 7, Figure 9A, B). An early diagenetic origin for the dolomite cement is indicated by: the displacive growth of the nodules - which preserve uncompacted sandstone grain fabrics, and; by the compactional deformation of nodules against each other and more competent quartz and feldspar grains (Figure 9A) – demonstrating that these features formed before significant burial. As with the eodiagenetic calcite nodules, the dolomite nodules have also been reworked as “detrital” grains along specific laminations in the sandstone, indicating that they also formed penecontemporaneously with the deposition of the Bunter Sandstone Formation. The dolomite nodules are micritic and microporous, and commonly display a concentric growth texture (Figure 7). However, the original structure may be obliterated to varying degrees by recrystallisation to (or replacement by) a coarser microdolosparite (Figure 6B, Figure 8), or by dissolution and partial replacement by later (mesodiagenetic) dolomite, ankerite, ferroan calcite or anhydrite (Figure 8).

Abundant dolomite occurs in the mudstones as a micritic or microcrystalline cement replacing the ferruginous clay matrix (Figure 9C, D), and cementing discrete laminae or forming irregularly-cemented horizons and nodules in mudstone (Figure 9C). The dolomite typically comprises aggregates of fine euhedral rhomb crystals. These can be finely growth-zoned with inclusion trails of nanoparticulate hematite (Figure 9D), with a dense intercrystalline matrix of hematitic clay. Similar dolomite also commonly cements and partially replaces red mudstone clasts (Figure 5), clay laminae and intergranular clay and silt matrix material in the sandstones.

This early dolomite was also seen to replace and overprint earlier-formed eodiagenetic calcrete fabrics in several wells across the study area (see above). It is later than the calcrete and therefore at least some of the dolomite in other wells may also represent dolomitised calcrete. However, in many cases it is not obvious that the dolomite replaces a calcite precursor (Figure 7), and the dolomite may therefore have precipitated directly as a micro-concretionary dolomicritic cement (i.e. dolocrete).

In rare instances there are discrete thin beds of dolosparite (e.g. well 48/10c- 11 at 2016.56 m). These comprise closely interlocking euhedral crystals of strongly compositionally zoned dolomite with no identifiable replacive textures, with evidence of reworking of coarse clasts. Some of these clasts are encrusted on their upper surfaces, suggesting possible algal coatings. These deposits may therefore be a primary dolomite precipitate, such as might form in an ephemeral lake or pond.

Distribution of the eodiagenetic carbonate nodules

Within the study sample set there is no stratigraphic control on the presence or abundance of the nodular carbonates. As well as being present in the various Volpriehausen members, they have also been recognised in the Bunter Shale and the Dowsing Formation. There is a regional variation, however; the highest nodule abundances were observed in samples from Quadrant 43 wells (43/12- 1, 43/15-B1 and 43/16- 1). *Fragmented* carbonate nodules were mostly observed within the LVS, an observation consistent with the higher energy depositional environment implicit in the coarser grain size of the sandstones from this member.

Origin of the carbonate nodules

Whilst their common framework grain disposition in the sandstone fabrics might suggest a purely detrital origin for these grains, several lines of evidence point to them having formed penecontemporaneously with deposition. In particular the observations showing nodule re-working, as well as the inclusion of nodule fragments as cores for other nodules. These features demonstrate that the nodules must be forming in the surface and near-surface, potentially with several periods of formation, mobilisation and re-deposition. Furthermore, the localised 'expanded' framework textures (Figure 6A, C, F) represents displacive nucleation and growth, which in turn indicates their formation in the sediment under minimal overburden. The bands of hematitic clay mark hiatuses in episodic calcite growth, with the clay layers either accumulating during periods of local re-mobilisation of the sediment (i.e. leading to layers of inherited clays) or through periodic infiltration under near-surface conditions (as described for other framework grains in section 4.2.1.1). For example, the hematitic clays observed trapped between and coating euhedral terminations to outer stellate calcite rims (Figure 5, Figure 6D) are strong evidence for *in situ* formation through infiltration. Similar overall features have been described from the onshore equivalent of the BSF (cf. Burley, 1984; Strong and Milodowski, 1987; Plant et al., 1999; Monaghan et al., 2012). These early carbonate fabrics are typical of pedogenic calcrete cements.

Some nodules partially enclose adjacent framework grains. Where these grains interrupt the clay rims and there is no evidence for nodule deformation (e.g. Figure 6I), this is taken as evidence for episodic calcite rim growth and clay rim formation through infiltration, *in situ*. The difference between displacive and inclusive nodule textures is likely be linked to the burial depth when the calcite formation takes place. Growth at a very shallow depth with low overburden, may give rise to displacive textures, whereas at slightly greater depths overburden may be high enough to inhibit displacive growth resulting in the development of nodules that include immediately-adjacent detrital grains. This in turn suggests that the period of *in situ* nodule development extended from eodiagenesis into early mesodiagenesis.

Although eodiagenetic calcrete cement is restricted in its present distribution, it may originally have been much more widespread. Calcrete nodules in some samples across the study area (Wells 44/23- 3, 42/25- 1, 41/18- 1), have been recrystallized and/or overprinted by later, deeper burial (mesodiagenetic), and commonly poikilotopic pore-filling calcite cement. This has produced patchy calcite-cemented areas of sandstone with an anomalously "expanded" or under-compacted grain framework, and displaying the "ghost" outlines of carbonate nodules defined by their original concentric infiltrated hematitic clay entrapped within the later calcite as evidence of their former existence. Similar "ghost" outlines are also present in the dolomite cements (Wells 41/18- 1, 42/25- 1, 43/12- 1, 44/23- 3, 44/23a- 10, 47/05- 1; Figure 8) and anhydrite (Wells 41/18- 1, 42/25- 1, 44/23- 3, 44/23a- 10, 47/05- 1; Figure 8), suggesting that the nodules may also have been partially replaced by these later minerals. The dolomite in these instances occurs

as fine euhedral rhombic crystals. Additionally, similar forms in non-ferroan micritic dolomite suggest possible early pseudomorphic replacement (see section below on early dolomite).

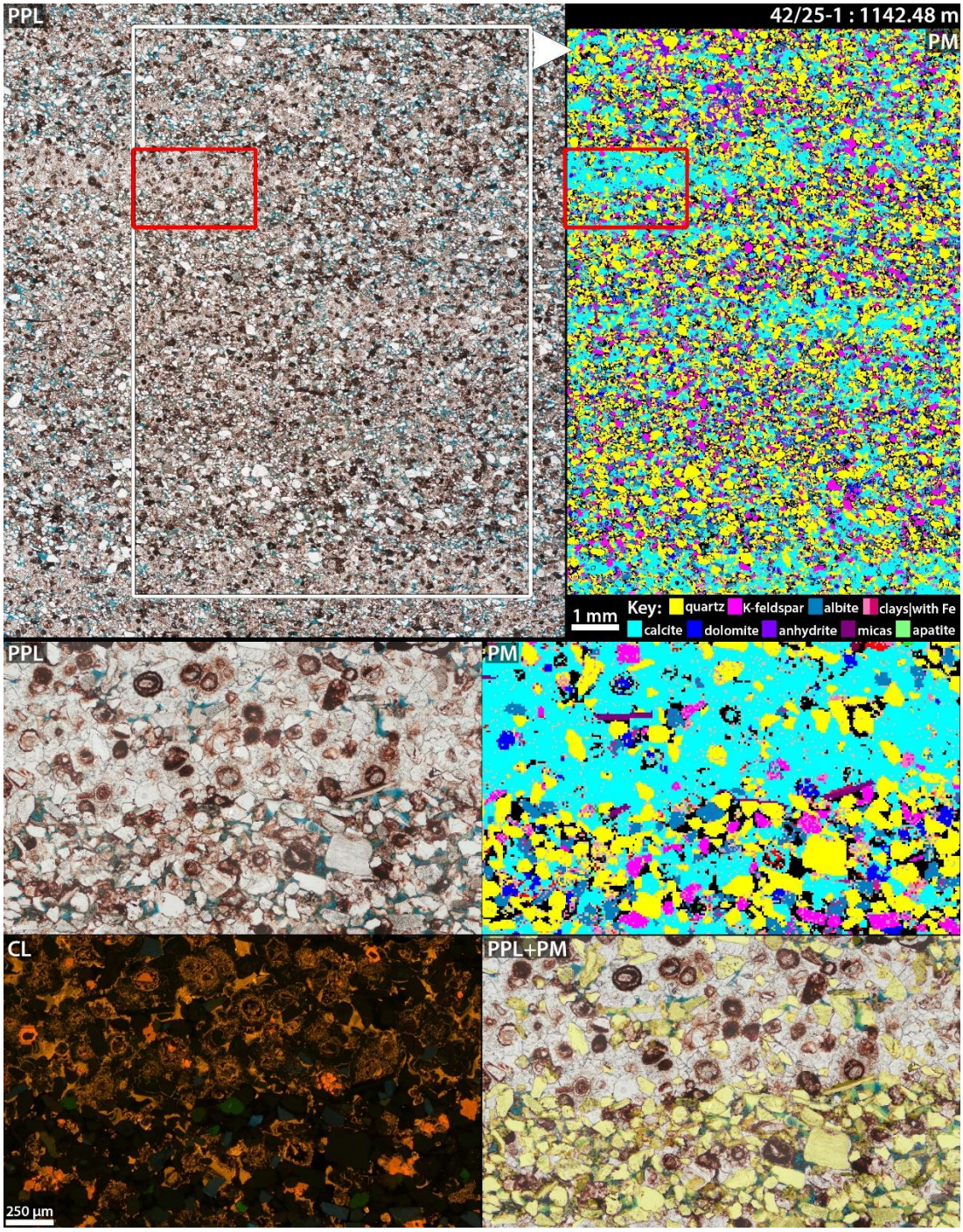

Figure 5: Calcite nodule enriched laminations, nodule internal forms, displacive calcrete cement. The top part of this figure shows a large area thin section in PPL and its associated phase map (PM), highlighting laminations enriched in calcite nodules (dark red grains in PPL, cyan in PM). The red boxed area is shown in detail in the 4 lower half images. The PPL quadrant (phase identifications in adjacent PM quadrant) shows a mm-thick calcrete layer (upper half) against a non-calcrete layer; both contain abundant hematitic clay defined nodules. Many nodules have hematitic clays trapped between and coating euhedral terminations to outer stellate calcite rims. The yellow overlay of detrital silicate grains in the PPL+PM quadrant highlights their widespread displacement by nodule-centred eodiagenetic calcite cement. In the CL quadrant, calcite shows pale orange, dolomite red-orange. Nodules have multiple concentric patterns, commonly with dark CL cores. Fringing and pore-filling cements, and overgrowths, have coarser oscillatory CL textures. Dolomite is a patchy cement locally replacing the calcite nodules. Sample details: top VCS, 42/25- 1, 1142.5 m, correctly oriented for way up.

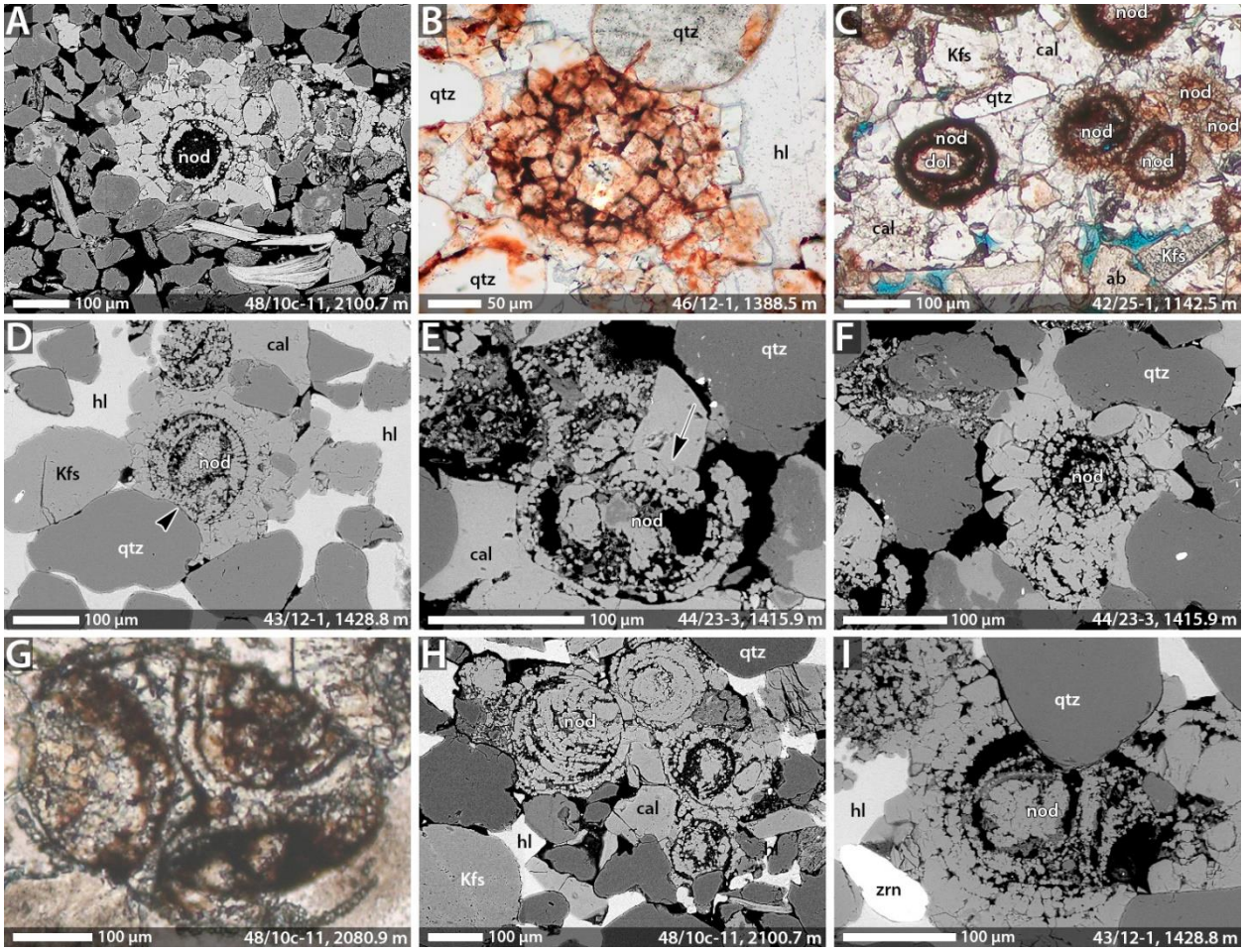

Figure 6: Characteristics of nodules (nod) from across the study area (well name and sample depths shown on individual images). BSE images except for B, C and G (optical PPL). Mineral identifications, from EDX data, are as follows: qtz – quartz, Kfs – K-feldspar, ab – albite, cal – calcite, hl – halite, zrn – zircon, dol - dolomite. (A) An expanded fabric developed associated with radial growth of calcite from the concentrically layered core. Note splayed mica flake at base. (B) A nodule replaced by dolomite rhombs; hematitic clays have no banded texture. (C) This lamination is mm-scale calcrete rich in calcite nodules; the expanded silicate grain fabric is associated with displacement by nodule-centred eodiagenetic calcite cement. Note diagenetic dolomite developed in a clay-rich nodule core. The nodules clustered to the right have hematitic clays between and coating euhedral terminations to outer stellate calcite rims. (D) A nodule with a core containing clays and a micritic intraclast. The inner layers are of uneven thicknesses with radial growth patterns. There is an expanded fabric associated with the fringing cement, except at one site (arrowed) where the nodule core has been compaction-deformed. (E) Compaction post fringing cement has driven (arrow) part of this nodule's rim into its porous core. (F) A partially expanded fabric associated with this nodule (to the left) is contrasted to partially enclosed grains to the right, with no evidence for any compaction deformation. (G) This rounded grain contains three well cemented nodule-like fragments. The degree of cementation and rounding contrasts with other locally reworked nodule fragments, so is more likely a lithic fragment, potentially from the Bunter Shale or other limestone source. (H) The core of the labelled nodule shows evidence of a reworked core in the form of truncated concentric rims. (I) A complex nodule core of mixed clay, silt and micrite has a well-defined concentric outer structure of coarsening calcite. There is no evidence of compaction around the part-enclosed quartz grain (cf. D), suggesting the enclosure is a result of *in situ* growth of the outer layers.

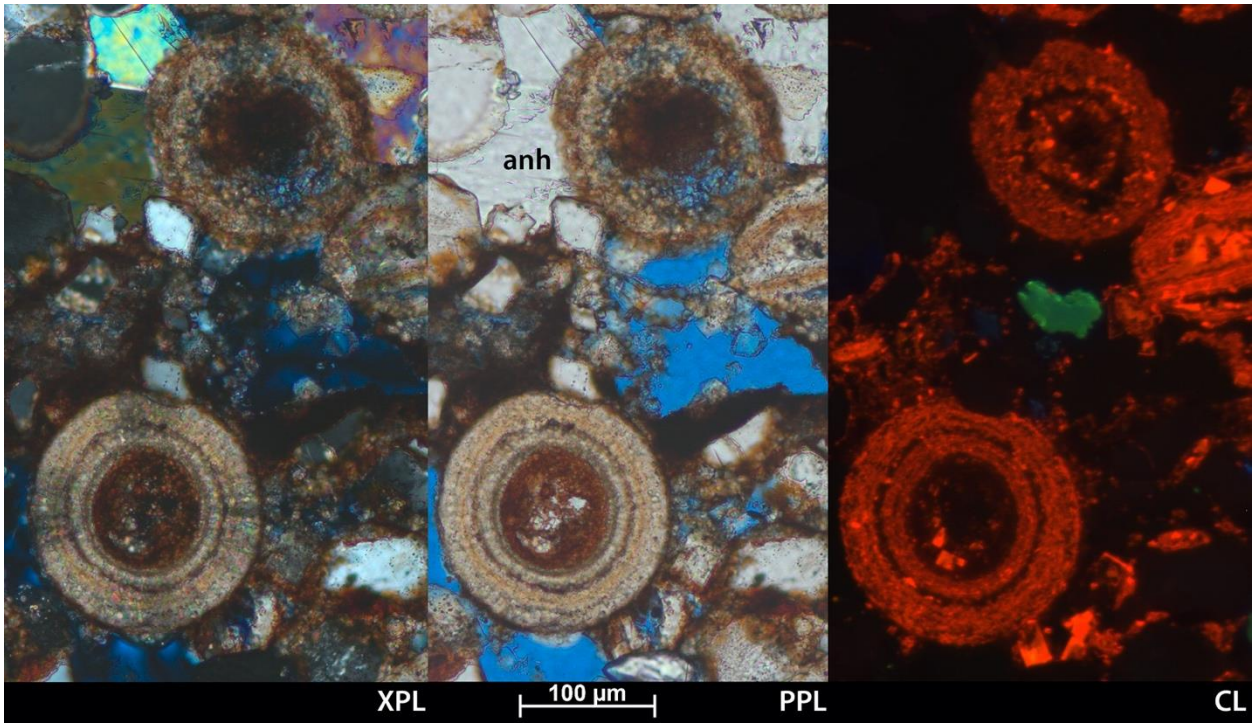

Figure 7: Detail of the structure, optical and CL characteristics, of dolomicritic nodules.
Showing the same field of view in XPL, PPL and CL for a cluster of micritic and microporous dolomitic nodules with well-developed concentric growth textures, locally cemented by anhydrite (anh) and intermixed with an infiltrated hematitic clay and dolomicrite matrix (mid VCS, 44/23- 3, 1374.8 m). One nodule (right edge of field of view) has a core with a planar structure defined by hematitic clay. Radial extinction in XPL highlights a radial growth pattern. The red CL colours suggest they are formed of Mn-bearing dolomite; coarser euhedral forms are in intergranular porosity and replacing the dolomicrite.

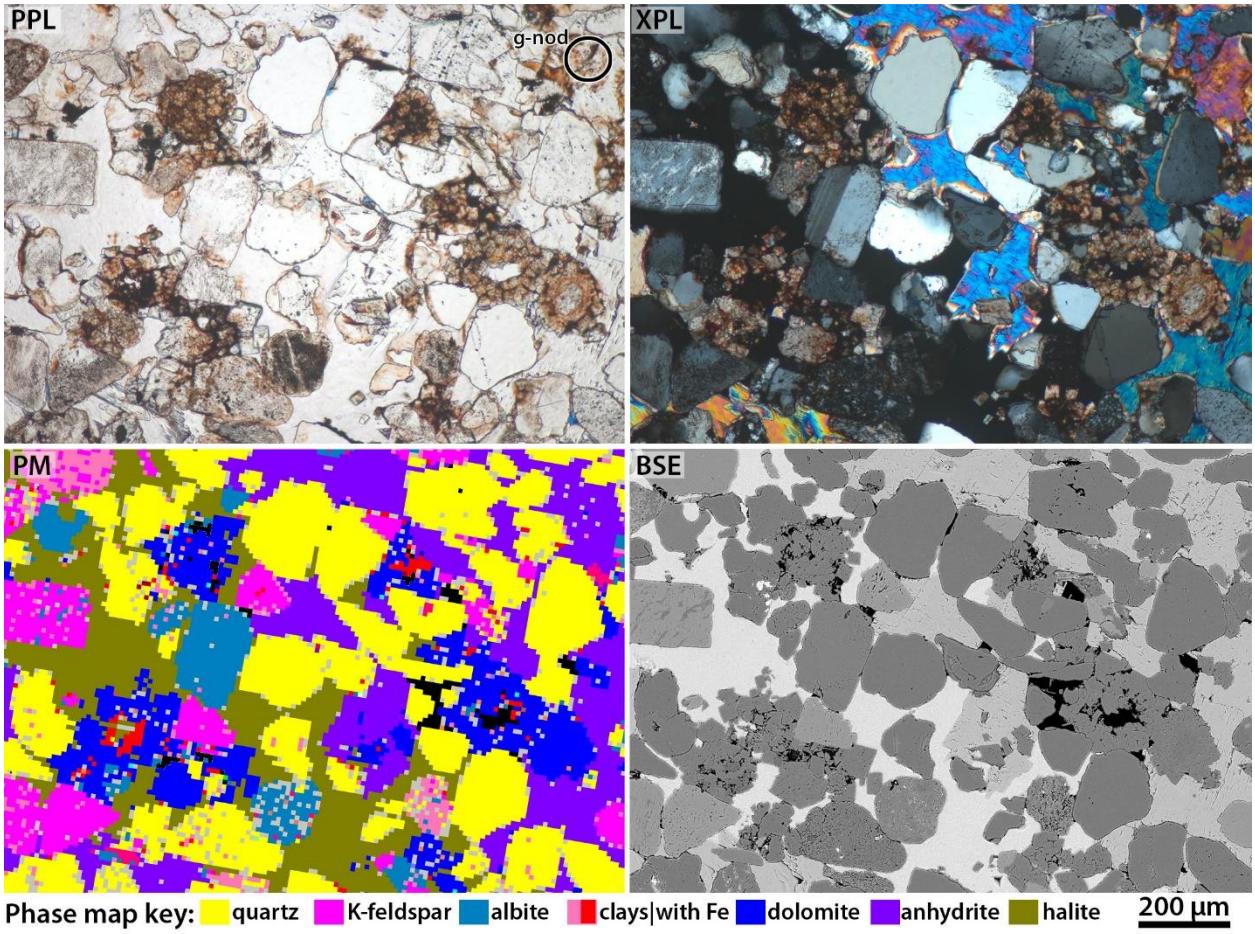

Figure 8: Features of dolomite-replaced carbonate nodules, halite-anhydrite cement intersection. Showing the same field of view in PPL, XPL and BSE (mid VCS, 43/12- 1, 1388.5 m) together with an AQM-derived phase map (PM – 10µm step size). The nodules are defined by hematitic clay rims mostly within rings and rounded patches of microdolosparite, which is probably replacive as indicated by poor preservation of internal structures. Local re-crystallisation of dolomite has given rise to a nodule outline enclosed within a single coarse crystal of dolomite (right edge). A 'ghost' nodule is evidence for anhydrite replacement (top right, g-nod in PPL). Anhydrite enclosed by halite is euhedral (centre), including some lath-like terminations.

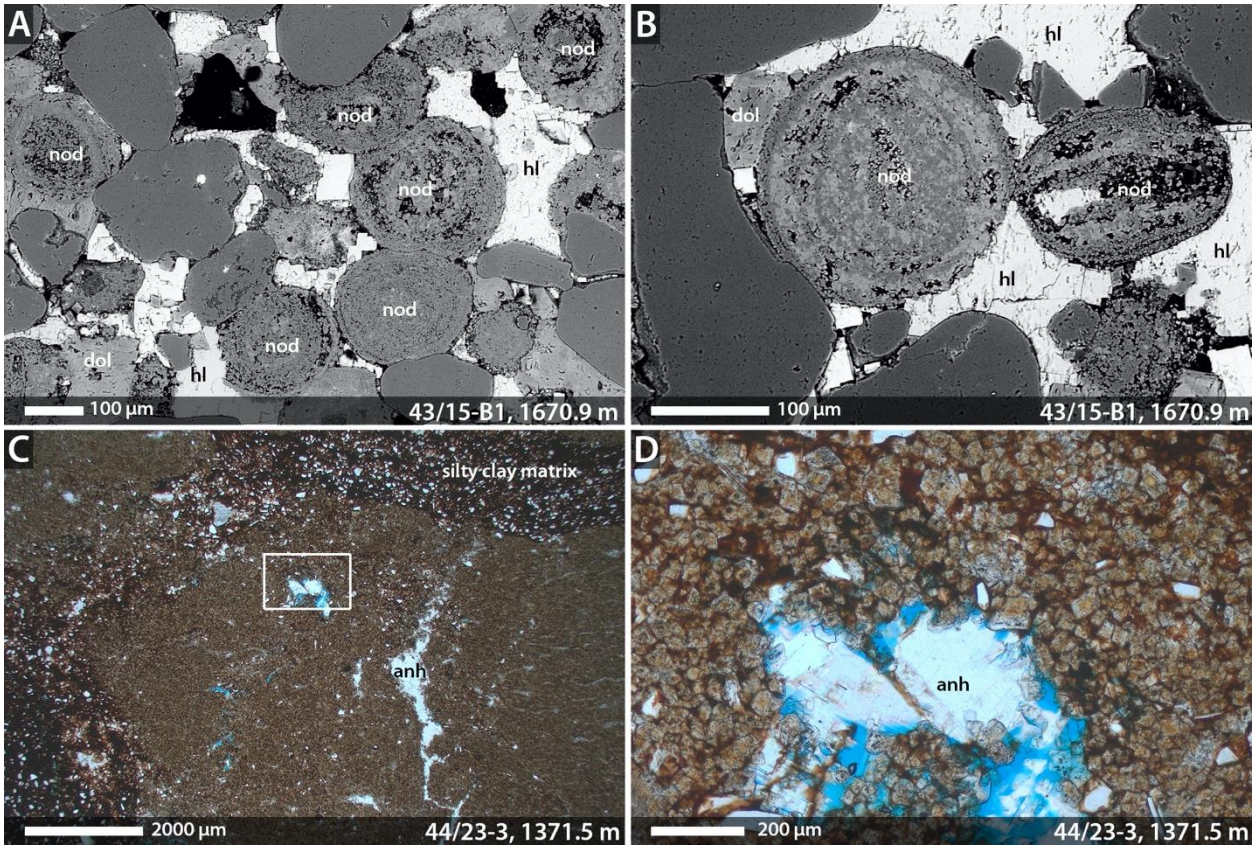

Figure 9: Features of dolomitic nodules (nod) and microcrystalline dolomite replacing clay matrix. A and B (mid VCS) are BSE images with phase identifications from EDX as follows: hl – halite, dol – dolomite. C and D (mid VCS) are PPL, D is from the boxed area in C. (A) Common dolomicritic nodules have well defined concentric textures. Here they form a significant part of the framework and show evidence of compaction deformation at grain contact sites. Halite and coarser dolomite occlude post compactional pore space. (B) Detail of the internal structures of some dolomitic nodules. (C) A ferruginous silty mudstone with fractured dolomitic patches, cemented by anhydrite (anh). Greater separation of silt grains in the dolomitic patch shows it formed displacively and / or pre-compaction. (D) Detail from C (boxed area) showing the dolomitic patches comprise fine euhedral crystals with inter- and intra-crystal hematitic clays. Well locations and sample depths are shown on individual images.

4.2.1.3 EARLY GYPSUM AND ANHYDRITE CEMENTS

Eodiagenetic anhydrite fabrics are major features of both the sandstone and mudstone lithologies, and are widespread across the basin.

In the mudstones, the anhydrite is commonly found as scattered concretions or nodules several tens of millimetres in diameter. They are particularly well-developed within the Intra-Solling Sand and Solling Claystone overlying the BSF in Well 43/15-B1 as well as in some of the mudstones in the VCS of Well 44/23- 3. The concretions have grown displacively, pushing the host sediment to the margins of the growing concretion to form nodules comprising almost pure anhydrite. These comprise a tight, dense, felted or aphanitic groundmass of fine anhydrite laths. Typically, the anhydrite is finer grained at the margins of the nodules but coarsens significantly towards the interior, indicating that recrystallization and progressive crystal growth at the expense of finer anhydrite has occurred as the nodules developed. Anhydrite formation can be so extensive in

some horizons that the original mudstone fabric has been completely obliterated, heaved-apart, irregularly-fractured and brecciated, by enterolithic masses of coalescing concretions (Figure 3F).

Relatively rare anhydrite pseudomorphs after gypsum were observed in some samples of both mudstone and sandstone. They display characteristically euhedral, acicular to bladed monoclinic crystal morphology (Figure 10A), and occur in stellate or radiating clusters (Figure 10B) that locally displace and disrupt the host sediment. These morphological forms of anhydrite are more typical of eodiagenetic gypsum similar to gypsum “desert roses”. Similar pseudomorphs were also observed enclosed within the aphanitic anhydrite groundmass of some mudstone-hosted anhydrite nodules, suggesting gypsum likewise formed as a precursor there.

Eodiagenetic anhydrite also occurs as local nodular cements in the sandstones but with a fabric that is quite different to that seen in the mudstones. This form of anhydrite is typically present in sub-spherical to lenticular patches of sandstone ranging from <0.1 to 20 mm diameter, varying from isolated and scattered nodules (Figure 3C) to abundant concentrations of anhydrite that can form locally well-cemented sandstone horizons. These cemented patches are differentiated from other anhydrite cements as they comprise interlocking fine (<50 µm) blocky crystals (Figure 10C, D) and preserve an uncompacted or expanded fabric of ‘floating’ detrital grains. This fabric demonstrates that the anhydrite is eodiagenetic since an absence of significant overburden is implicit in these textures. Outside these nodules the sandstone cemented by anhydrite is typically more compacted and the anhydrite is present as a poikilotopic cement that can enclose (and therefore post-date) the nodules (Figure 10C, D); this mesodiagenetic anhydrite is further characterised below.

The displacive crystallisation of the anhydrite (or its gypsum precursor) in both the sandstone and mudstone lithologies indicates mineralisation occurred under very limited overburden and therefore before significant burial. However, it largely post-dates early calcite and dolomite mineralisation since the eodiagenetic carbonate mineral fabrics are often entrained within the anhydrite cement. However, some anhydrite nodules completely exclude carbonates (44/23- 3; 1442.5 m), suggesting locally it formed before or penecontemporaneous with the carbonates.

These early nodular diagenetic anhydrite and gypsum fabrics closely resemble those described from both modern and ancient sabkha environments (e.g. Shearman, 1966; Butler, 1969; Kinsman, 1969; Dean et al., 1975; Testa and Lugli, 2000). Similar anhydrite fabrics are also very well-developed in the Mercia Mudstone Group onshore in the East Midlands, UK (Milodowski and Rushton, 2008).

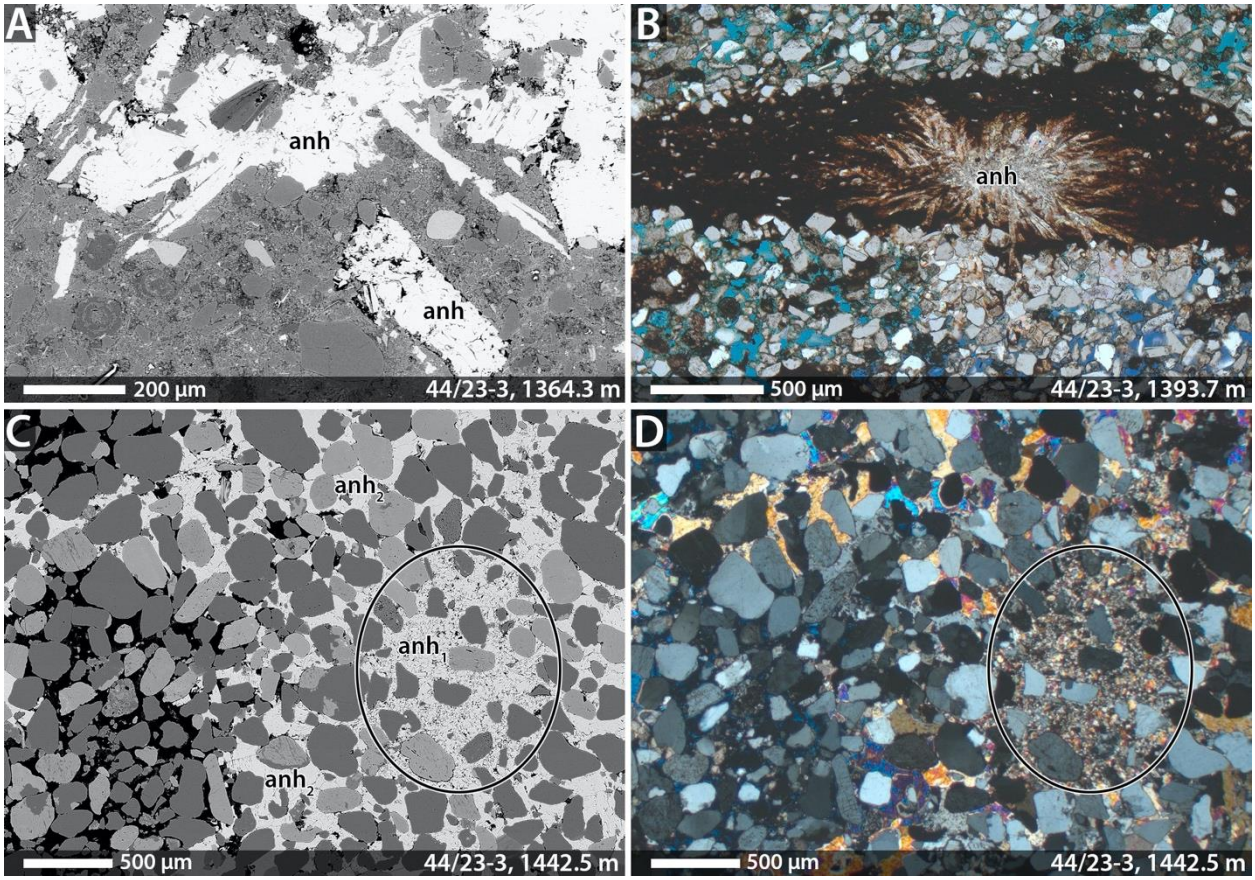

Figure 10: Anhydrite cementation, with evidence of pseudomorphic and pre-compaction formation. A (mid VCS) and C (top LVS) are BSE images, B (mid VCS) is optical PPL, D (top LVS) is optical XPL covering the same area as C.
(A) Anhydrite (anh) is present within a silty mudstone interval displaying blocky (lower right) and acicular, bladed (above centre) forms. The latter are conjectured to be replacive after gypsum. (B) A radial cluster of acicular anhydrite (anh) is present in a mudstone lamination interbedded with sandstone. This morphology is indicative of an eodiagenetic gypsum precursor. (C & D) This image pair shows two texturally discrete forms of anhydrite. The encircled area contains a nodule of finely crystalline anhydrite (anh_1, note finely speckled extinction pattern in D) with an 'expanded' grain fabric suggesting pre-compaction formation with an element of displacive formation. The surrounding sandstone has a variably compacted texture and is cemented by poikilotopic anhydrite (anh_2). Notched and embayed margins in the left of this field of view indicate some anhydrite dissolution has occurred. Well name and sample depths shown on individual images.

4.2.1.4 PEDOGENESIS

Heterogeneity in grain packing is a characteristic widespread in the sandstones of the study area, evident at a millimetre scale both within and outside of the eodiagenetic cemented patches in some of the sandstones. Consequently, at least some of these textures must have eodiagenetic origins. Sub-millimetre domains of both close-packed aggregated sand grains - in some cases enriched in infiltrated clays and in eodiagenetic carbonate nodules - and relatively uncompacted sand, commonly occur in close proximity. This finer-scale fabric bears some resemblance to the aggregation of particles observed during pedification (e.g. Bradeau *et al*., 2014; Milodowski *et al*., 2015), and may therefore represent the incipient development of a soil fabric prior to anhydrite cementation.

4.2.2 Mesodiagenesis

4.2.2.1 Quartz and feldspar overgrowths

Minor to trace amounts of authigenic quartz, K-feldspar and albite are present in the sandstones. They occur as syntaxial overgrowths on detrital quartz and feldspar grains (Figure 11A), respectively, locally interlocking to form a rigid grain framework. However, these authigenic overgrowths have little volumetric impact on the intergranular porosity. They are absent on detrital grains enclosed within eodiagenetic calcite, dolomite and anhydrite cements, demonstrating they post-date these early carbonate and sulphate cements. Grain overgrowths are affected by compaction but may also occur locally grown around compacted grain contacts. This implies that the quartz and feldspar authigenesis occurred during ongoing burial compaction. Authigenic quartz, and feldspar intergrowths are also closely associated with framework grain dissolution sites (after felsic lithic fragments and some detrital feldspar grains), where they occur as both internal and external overgrowths, or grain replacements. Albite was also identified as a rare partial replacement of calcite eodiagenetic nodules (Figure 11B). Albite overgrowths are best developed in Block 41 samples.

4.2.2.2 Dolomite dissolution

Some of the eodiagenetic euhedral dolomite shows evidence of partial dissolution. This is in the form of intracrystal pores, preferentially developed in specific growth zones (Figure 11D), and corroded margins subsequently overgrown by later dolomite (Figure 11C). It is not possible to be precise about the timing of the dissolution.

4.2.2.3 Dolomite-ankerite cementation

Ferroan dolomite and ankerite are common in many of the sandstones, characterised by euhedral pore-lining and -filling rhombic crystals that are commonly strongly compositionally zoned (Figure 11C, E, F). They are commonly formed as syntaxial overgrowths on earlier (eodiagenetic) non-ferroan cores (Figure 11F), particularly on eodiagenetic dolomite in mud rip-up clasts, also as neo-formed crystals with ferroan cores and outer zones; varied iron contents are typical, with highest iron contents commonly associated with the outermost zones, some of which are compositionally ankerite. Some of these zoned dolomites, however, have low iron contents in their outer rims (Figure 11E, F). These ferroan dolomites show identical growth zone structures and crystal forms outside and inside poikilotopic anhydrite cements (Figure 11E, F), but are absent from eodiagenetic anhydrite nodules (and sites where anhydrite nodules have been replaced / recrystallised).

Ferroan dolomite-ankerite mineralisation is locally abundant as a patchy intergranular cement between compacted sand grains, or as scattered isolated rhombic crystals. It also locally replaces eodiagenetic dolomite fabrics and can be seen filling framework grain dissolution sites after detrital feldspar and lithic grains. In combination, these mineral and textural relationships show that the ferroan dolomites formed relatively early during mesodiagenesis.

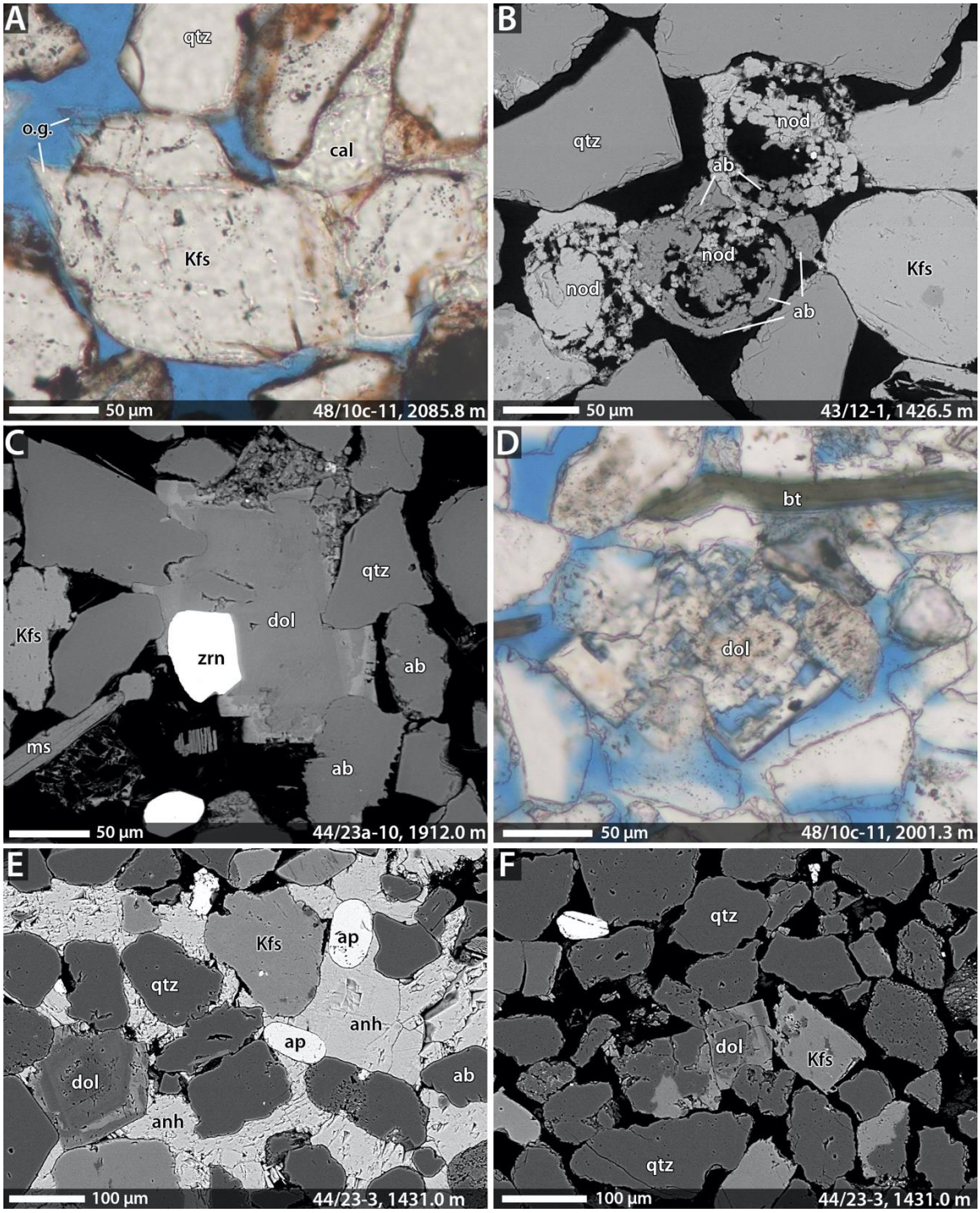

Figure 11: Mesodiagenesis of feldspars and dolomite in sandstones.
A (top LVS) and D (mid VCS) are optical PPL, whilst B (top LVS), C, E and F (all base VCS) are BSE images. Phase labels are: qtz – quartz, ab – albite, Kfs – K-feldspar, zrn – zircon, ms – muscovite, ap – apatite, bt – biotite, dol – dolomite, anh – anhydrite, nod – nodule. (A) A K-feldspar grain with minor saw-tooth-like overgrowths (o.g.) that have formed over the red-brown grain-coating clay. (B) Calcite nodules in framework grain positions in the sandstone fabric have been partially altered to albite. (C) A dolomite with concentric growth zones (centre; brighter zones are richer in iron) has cemented detrital grains. The non-euhedral and embayed outline to one of the zones shows there was an episode of dolomite dissolution prior to the final growth episodes. (D) The central dolomite has intracrystal pores, evidence of post-formation dissolution. (E&F) Dolomite crystals with growth zoning from the same sample within (E) and without (F) anhydrite cemented areas. The outermost zones of both are similar (BSE dark on a brighter zone),

showing that it formed prior to anhydrite formation. Well name and sample depths shown on individual images.

4.2.2.4 ANHYDRITE CEMENTATION

Anhydrite is a major mesodiagenetic cement in the sandstone lithologies (e.g. Figure 3B). In contrast to the eodiagenetic anhydrite, much of this later anhydrite cement is present as a poikilotopic intergranular cement (Figure 10C, D). A widespread characteristic associated with this anhydrite is textural heterogeneity.

The anhydrite occurs as an intergranular cement in sandstone volumes displaying close-packed detrital grain fabrics (common long-edge, rare sutured contacts; Figure 11E, Figure 12A, F), fills compaction-induced point-contact stress-cracks in detrital grains (Figure 12A) and irregular fractures formed by the compaction of eodiagenetic carbonate nodules, and encloses plastically-deformed grains such as micas and mudstone clasts. Fully developed calcite and dolomite cements are also enclosed by the anhydrite (Figure 12A, E). These observations show that this anhydrite cementation was coeval with, and / or post-dated, significant burial compaction and the other major diagenetic cements, apart from halite.

The textural heterogeneity of the enclosed framework grains is shown by the common observation of oversized areas of apparently grain-free anhydrite cement, many of which are part of the same poikilotopic crystals that cement compacted framework textures (Figure 12A, B, E). Some of the grains that are cemented at the margins of these oversized areas have noticeably looser fabrics, either 'floating' or with only simple point contacts. This fabric is typical of framework grain dissolution and replacement (Schmidt and McDonald, 1979b). Corroded relicts of grains and inclusion outlines of hematitic clays (Figure 12B) within the oversized intergranular anhydrite areas support this model. Grain relicts of feldspar and lithic framework grains show these as grain types being replaced. The presence of residual hematitic rims further indicates eodiagenetic carbonate nodules as being replaced in some instances. Some oversized areas have no grain remnants or hematitic rims, and the overall grain fabrics are similar to those observed around eodiagenetic anhydrite nodules (anh_1 in Figure 10C, D); for these instances it is suggested that the mesodiagenetic anhydrite has formed through recrystallisation or replacement of the eodiagenetic anhydrite.

Anhydrite was also observed filling narrow vertical fractures in sandstone units within the Solling Claystone (Figure 12C). The fractures also display a concentration of anhydrite cementation within the sandstone immediately adjacent to the fractures. This shows that some anhydrite mineralisation also accompanied minor tectonic fracturing events and that the fractures have acted as conduits for the anhydrite-mineralising fluid.

There is some evidence for at least two episodes of mesodiagenetic anhydrite cementation. The fracture-fill noted above is an example of this, as the fracturing has affected sandstone already partially cemented by anhydrite. In some samples, quartz overgrowth is better developed outside poikilotopic anhydrite cement, whereas in others it is equally developed inside and outside.

Whilst most anhydrite displays growth forms, with euhedral crystal faces in contact with other cements and porosity, there is some evidence of localised dissolution in the form of notched and embayed margins (44/23- 3, 1442.5 m; 44/23- 3, 1405.4 m; Figure 12D). Similarly notched anhydrite is also present enclosed by and as inclusions within poikilotopic halite cement (Figure 12F). This shows that dissolution of some anhydrite must have occurred during later mesodiagenesis, prior to the precipitation of the major halite cement. However, there are also instances where secondary porosity from anhydrite dissolution has formed after being enclosed

within halite cement. It is possible that some of the observed anhydrite dissolution, particularly where halite is also partially dissolved, could have occurred during the original coring, through post-coring handling (e.g. plugging, slabbing) and / or during storage.

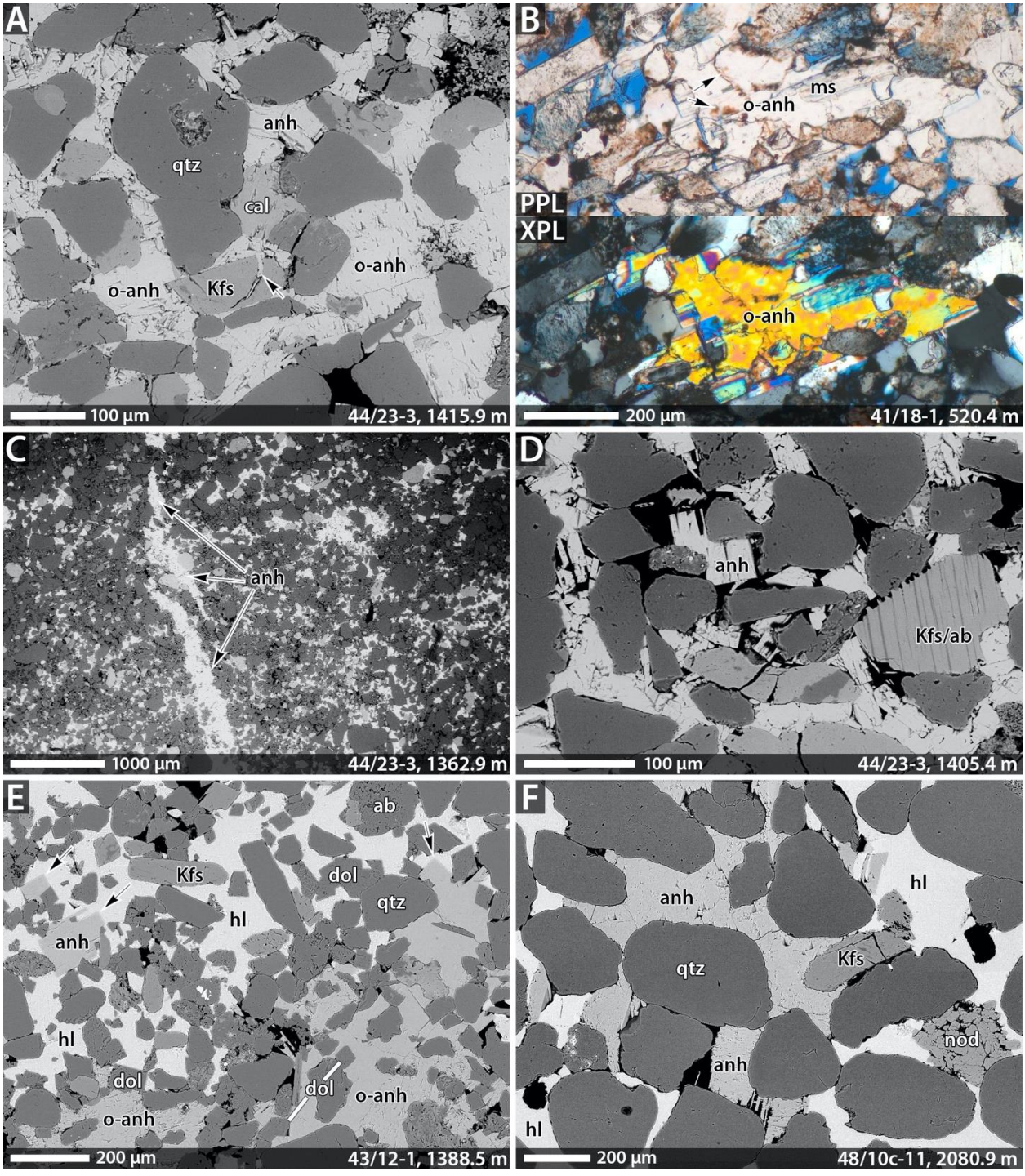

Figure 12: Textures and associations relating to mesodiagenetic anhydrite.
All BSE except B which is a matched pair of optical PPL and XPL images. The samples are from mid VCS except C, which is SC and F, which is top LVS. Phase labels are: anh – anhydrite, hl – halite, qtz – quartz, cal – calcite, ab – albite, Kfs – K-feldspar, dol – dolomite, ms – muscovite. (A) Poikiotopic anhydrite encloses calcite and has cemented a well-compacted framework grain fabric, including a compaction-induced grain fracture (arrow). Textural heterogeneity is shown in areas of apparently expanded grain fabric represented by oversized anhydrite (o-anh). (B) Ghost grain shapes are discernible within this oversized anhydrite in the form of relict hematitc clay rims (arrowed in PPL), indicative of grain replacement. (C) An example of anhydrite-cemented

fracturing (arrowed). The fracture is an *en echlon* set in sandstone, cemented by carbonate and anhydrite. (D) In this area of anhydrite cement, partial dissolution of the anhydrite, preferentially along cleavage planes, is shown by notched edges of the anhydrite exposed to the porosity. (E) The framework grain fabric shows considerable heterogeneity, with oversized anhydrite areas (o-anh) associated with 'expanded' areas. Anhydrite enclosed by halite shows euhedral crystal forms (arrows). Dolomite is similar in both halite and anhydrite cement, but is absent in the oversized anhydrite areas. (F) In contrast to E, anhydrite here has notched margins from dissolution, including edges enclosed by halite. Well name and sample depths shown on individual images.

4.2.2.5 HALITE CEMENTATION

Halite is present as a mesodiagenetic cement in many of the sandstones in the study area, and is developed as a major cement in some parts of the BSF sequence, completely to nearly completely occluding intergranular porosity in some samples. It occurs predominantly as a poikilotopic intergranular pore-filling cement (Figure 13, Figure 14), also as an intragranular cement in microporous detrital grains (eodiagenetic carbonate nodules (Figure 14C), partially altered and dissolved silicate grains).

As with the anhydrite, sandstones cemented by halite generally display some heterogeneity in framework grain packing. Halite largely cements rock volumes with close-packed grain frameworks (common long-edge, rare sutured contacts) and in these rocks halite can also be seen to fill compaction-induced stress-cracks in detrital grains (Figure 14B, C) as well as enclosing compactionally-deformed detrital grains. However, there are also areas where halite occupies oversized areas and where grains display looser packing ('floating' grains, point contacts; Figure 12E, Figure 14B), although not to the same extent as anhydrite. This fabric is typical of framework grain dissolution and replacement (Schmidt and McDonald, 1979b). Corroded relicts of grains and inclusion outlines of hematitic clays support this model. Feldspar and lithic framework grains show these as grain types being replaced. The presence of residual concentric hematitic rims further indicates eodiagenetic carbonate nodules as being replaced in some instances.

As described above, halite paragenetically post-dates anhydrite cementation, with anhydrite typically found enclosed in the halite cement. In some instances, the enclosed anhydrite is notched and corroded (Figure 12F), suggesting pre-halite dissolution or replacement by halite during formation. However, in most cases the anhydrite enclosed within halite has euhedral crystal terminations (Figure 12E). It is concluded, therefore, that intergranular halite has largely not formed in the place of anhydrite. Similarly, halite cements enclose most other diagenetic cements, including eodiagenetic calcite (Figure 14A, B) and mesodiagenetic dolomite (Figure 8). K-feldspar and quartz overgrowths have also been enclosed by halite.

In some laminated sandstones with strong grain size contrast, halite preferentially cements the better-sorted, coarser-grained laminations. Virtually complete halite cementation has only been observed in sandstone bodies and laminations with grain sizes coarser than very fine sand (Figure 13A, B). In these instances, halite exposed to residual pores exhibits euhedral faces (Figure 14A, B). These euhedral terminations show that the grain-size preference is related to the growth of halite. Not all fine to coarse grained sandstones are cemented by halite; therefore, grain size is not the only determinant for halite cementation.

Where halite exposed to porosity has notched, embayed and porous margins (Figure 14C), this is taken as evidence of dissolution. This evidence was observed in many of the sandstone samples examined. It is recognised that, due to the legacy nature of many of the samples, some

of these fine-scale dissolution textures could have occurred during the original coring, through post-coring handling (e.g. plugging, slabbing) and / or during storage. Similarly, thin pore-rimming patches of halite may be post-coring drying precipitates. However, dissolution textures developed on a more widespread scale are more likely 'true' halite textures. Amongst these textures are instances where significant porosity is present in specific laminations of an otherwise fully cemented sandstone sample (Figure 13C) with the porosity-exposed halite having dissolution textures; notched and embayed textures as well as being present in only the narrowest pores (Figure 14D). These halite dissolution textures are observed in the coarsest grained laminations, showing that dissolving fluids are penetrating along laminations with the largest potential pore size network.

Consequently, both cementation and dissolution of halite cement show distributions in part controlled by detrital grain sizes.

Halite was also found as vein / fracture mineralisation in localised fracture zones near-perpendicular to bedding. Two contrasting examples were observed in mid VCS in Well 43/16-1 (945.6 m) and in mid LVS in 48/10c- 11 (2121.7 m). These occurrences display contrasting relationships between the vein-filling halite and the adjacent wallrock. In the former, which is a very fine-grained sandstone, there is no penetration of halite into the sandstone, whereas in the latter, in which the fracture affects a medium grained sandstone, halite cement centred on the fracture has penetrated a few mm into the porous part of the sandstone. It is likely that the first case is an example of halite cementation being confined to the fracture by the same grain size constraints as have been observed for the general cementation. Similarly, the second case, with the coarser grain size, fits the same pattern of preferential halite cementation. Additionally, in the second case, the fracture in question has affected existing halite cementation that is residual after partial dissolution (again, some grain size preference is shown in the dissolution), showing that both the fracturing and fracture-related halite cementation have occurred after halite cementation and partial dissolution in the sandstone.

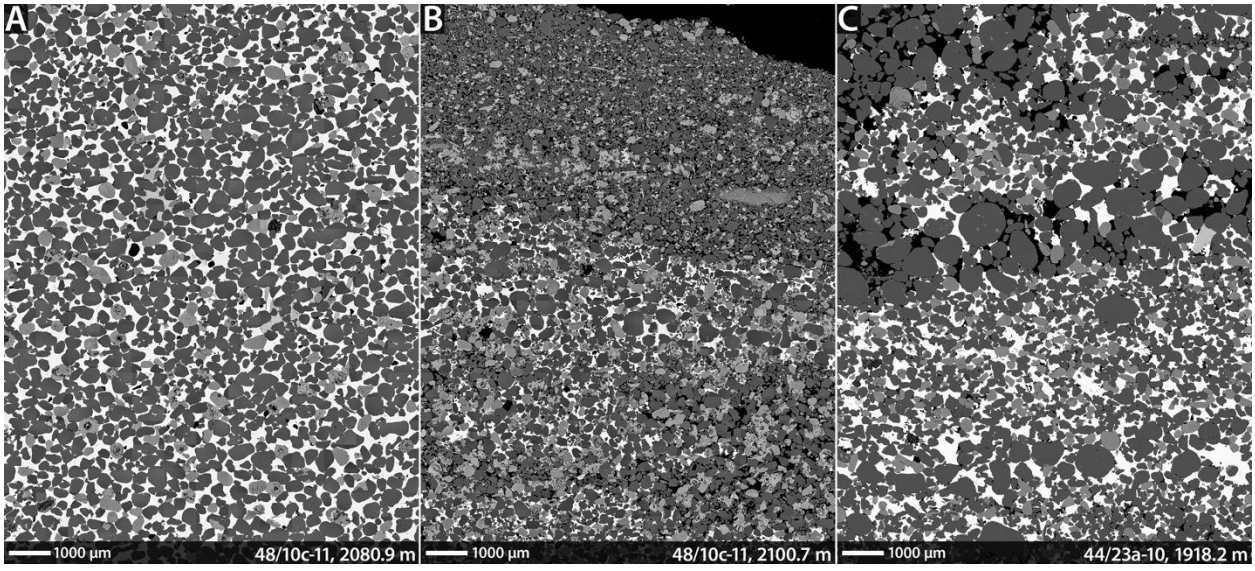

Figure 13: Lamination-scale variation of major halite cementation.
Mosaiced multi-tile BSE images in which halite cement is the brightest phase. All are top LVS. (A) A well sorted medium grained sandstone fully cemented by poikilotopic halite. (B) A finely laminated very fine, fine, and medium grained sandstone in which halite preferentially cements the coarser grained laminations. (C) A laminated fine to coarse grained sandstone. The finer grained laminations are completely cemented by poikilotopic halite, but the coarsest are not.

Halite exposed to macropores has rounded and embayed edges, indicative of dissolution. Well name and sample depths shown on individual images.

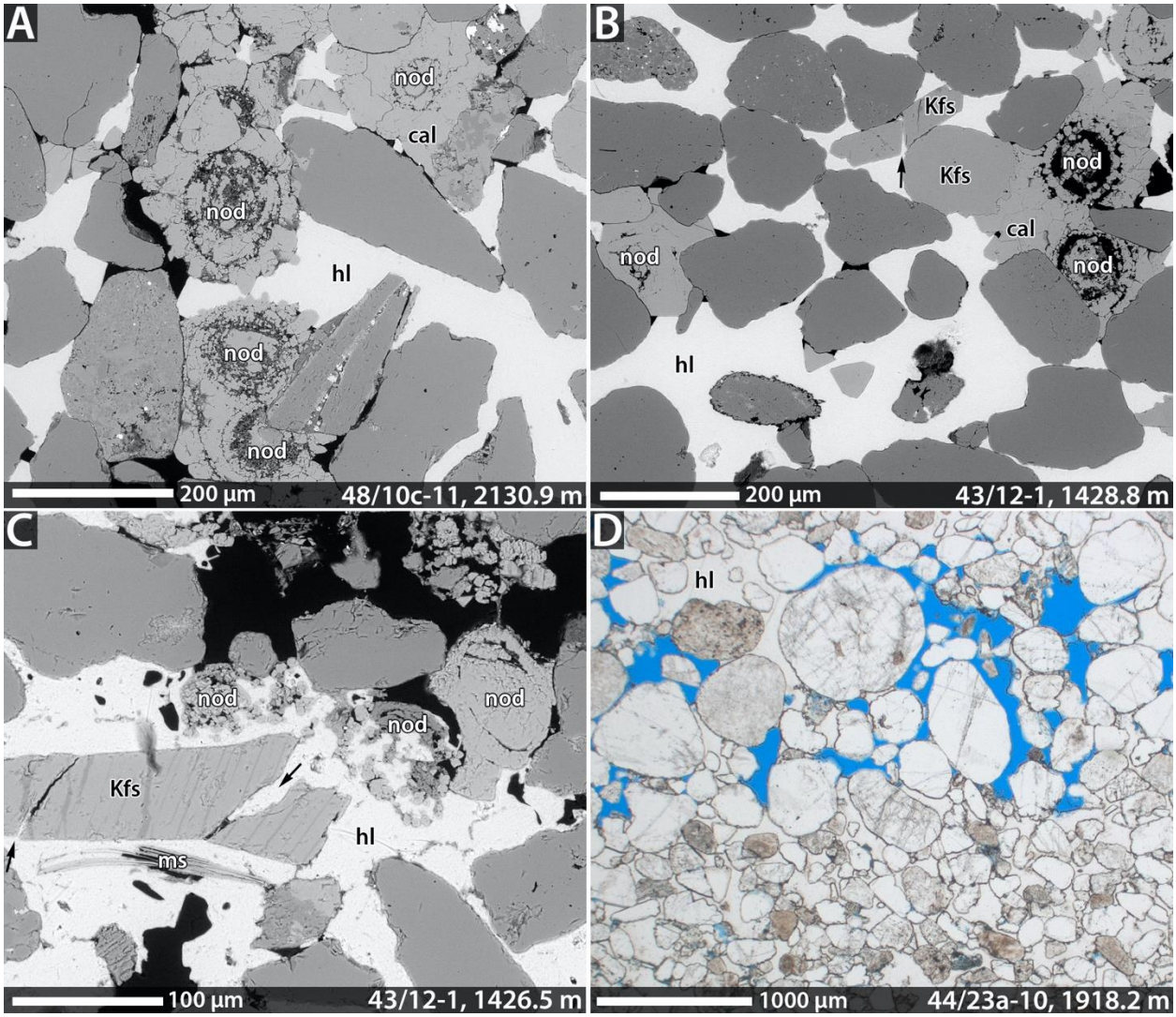

Figure 14: Pore-scale features of halite cementation.
BSE images except for D, which is optical PPL. A is mid LVS; B, C, D are top LVS. Phase labels are: hl – halite, cal – calcite, Kfs – K-feldspar, ms – muscovite, nod – carbonate nodule. (A) This fine-grained sandstone is well cemented by halite, which displays euhedral terminations (left) against residual porosity. Calcite overgrowths enclosed by the halite have euhedral terminations. (B) Also well cemented by halite, this fine-grained sandstone has a heterogeneous fabric with an open grain fabric at the base and a compacted fabric at the top, including a grain-contact induced grain fracture cemented by halite (arrowed). (C) Halite cement here again has formed in compaction-induced fractures (arrows) and has also occluded intragranular micropores associated with eodiagenetic nodules. Notched, porous and embayed margins to halite are evidence of its partial dissolution. (D) Detail from Figure 13C. Halite fully cements the fine and medium grained laminations, but the coarse-grained lamination is porous (blue). The halite distribution is residual after partial dissolution, bridging the narrowest pores and with embayed margins. Well name and sample depths shown on individual images.

4.2.2.6 FERROMANGANOAN CALCITE CEMENTATION

Late-stage ferromanganoan calcite is observed as a minor component in many of the sandstones but may be locally important as a major pore-filling cement. It is excluded from most areas

cemented by anhydrite and halite. It occurs as a poikilotopic intergranular cement and as late stage euhedral overgrowths on earlier calcite. This calcite also rests on etched and corroded halite or anhydrite cement surface, and in some cases appears to partially replace anhydrite. The calcite itself shows no evidence of dissolution and typically forms euhedral crystal faces where exposed in open pores.

4.2.2.7 MINOR AUTHIGENIC MINERALS

Trace amounts of authigenic kaolinite were observed in some sandstones. It occurs as book-like or vermicular crystals, usually associated with framework grain dissolution sites after probable feldspar or felsic lithic fragments, or partially filling intergranular pores adjacent to framework grain dissolution sites. In some cases, the kaolinite appears to be closely associated with and may be partially enclosed within, the late ferromanganoan calcite cement. This would suggest that kaolinite formation is not related to dilute meteoric water flushing during uplift and telodiagenesis, as is seen at outcrop in the equivalent onshore sandstone sequence (e.g. Burley, 1984; Bath et al., 1986; Strong and Milodowski, 1982; Monaghan et al., 2012). Rather its association with ferromanganoan calcite would suggest that it may have been deposited from reducing pore fluids possibly associated with decarboxylation of organic matter and hydrocarbon movement during deep burial diagenesis.

Traces of fibrous illite were found lining open porosity in some sandstones. The illite is nucleated on eodiagenetic and inherited clay pellicles coating detrital grains. It is rarely nucleated on the edges of authigenic kaolinite plates. In these cores the illite fibres are broken and collapsed onto the poor walls as a result of core-drying after drilling. Fibrous illite is very susceptible to collapse and damage during core handling after drilling, and it is often missed or underestimated in petrographic studies unless specialised core preservation strategies have been employed (cf. McHardy et al., 1982). It has been identified as an important phase affecting the permeability in the Sherwood Sandstone Group (BSF equivalent) onshore in the Cleethorpes geothermal well (Milodowski *et al*., 1987; Monaghan et al., 2012).

Barite was identified in minor to trace amounts as a late-stage cement in the VCS in wells 42/25-1, 43/12- 1, 44/23- 3 and 48/10c- 11. It occurs as a poikilotopic intergranular cement, locally replacing or resting on corroded anhydrite, also occluding oversized intergranular pores that are characteristic of secondary framework grain dissolution sites (Schmidt and McDonald, 1979b) and of sites where displacive eodiagenetic cements have been replaced.

An authigenic Na-Ca zeolite-like mineral was tentatively identified in only one sample of sandstone from the VCS in Well 43/16- 1 (937.41 m). The zeolite-like phase is clearly hydrous (being easily damaged by the electron beam during BSE observation), and occurs as a grain-replacement or infilling framework grain dissolution sites, after some felsic grains. Its precise position within the diagenetic evolution is unclear. It post-dates compaction, and encloses (and therefore also post-dates) ferroan dolomite-ankerite cement. However, its relationship to other mesodiagenetic features could not be ascertained.

Analcime was identified as rare pore-filling euhedral equant crystals up to 50 µm across in Well 43/12- 1 (1391.87 m); the identification was confirmed by XRD. Analcime has previously been identified as a minor diagenetic constituent of equivalent strata in the North German Basin (Weibel and Friis, 2004) where its formation has been associated with the influx of saline brines. No paragenetic relationships were observed for this phase in this study.

4.3 CONTROLS ON POROSITY AND PERMEABILITY IN THE BUNTER SANDSTONE

4.3.1 Primary porosity and compaction

One of the defining properties of the BSF in the UKSNS is the common high abundance of diagenetic cements. Some of these cements are penecontemporaneous with deposition and the locally common concretionary nodules are effectively (at least in part) framework grains. Because nodule mineralogies are also major intergranular cements (carbonates, anhydrite), and these nodules have commonly been overgrown and / or replaced, the identification of the primary grain structure of the sandstones is considerably complicated, as is recognition of their primary porosity.

Where determined, petrographically calculated minus-cement primary porosities are, in most cases, similar to estimated theoretical porosities at the current burial depth (Table 3, using the generic compaction curves for the North Sea values from Ramm and Bjorlykke, 1994). The calculation of these minus-cement porosities is complicated by the difficulty in identifying cemented primary porosity because of the abundant diagenetic replacement mechanisms of framework grains identified and described above. This is particularly relevant where the previous presence of eodiagenetic carbonate nodules is only possible to identify by sparsely distributed relict silicate components such as the clay rims. This introduces a relatively high level of uncertainty in the calculations. However, qualitative observations of the sandstone fabrics in the samples from the central North Sea do support this deduction; most of the samples have a degree of compaction that is in equilibrium with current burial depth, irrespective of the degree of cementation. The main exception to this is the samples from near-shore locations (41/18- 1, 42/25- 1) where silicate cements dominate or are more common, and compaction is more strongly developed than in most of the centrally located samples.

A feature that is observed throughout the sandstones of the study area is the common presence of small scale (millimetre) variations in the degree of compaction. This small-scale patchy fabric was observed across the study area and in all formation members.

Where there are eodiagenetic carbonate or sulphate cements it is common for the framework grain fabric to be uncompacted or even appear expanded. However, some of this appearance comes from the fact that the eodiagenetic carbonate nodules were either part of the framework grain fabric or formed in the immediate subsurface with negligible overburden. Subsequent replacement of these nodules by later cements, as is evidenced by their ‘ghost’ fabrics in carbonates, anhydrite (Figure 12B) and halite, suggests that some of the apparently expanded fabrics may be due to the complete replacement of nodules, where even the clays and hematite that form the ‘ghosts’ have been eradicated. Other expanded fabrics are more obviously related to eodiagenetic cement formation in both sandstones and mudstones, as has been described above.

The same scale of compactional fabric variation was also observed where there are mesodiagenetic cements, in particular halite and anhydrite. These enclose expanded fabrics, poorly compacted fabrics and well compacted fabrics, with the last illustrated by cemented grain clusters with long edge and sutured contacts, and compaction-fractured grains (Figure 14B, C). This patchy fabric was observed to be similarly developed in the partially cemented sandstones both inside and outside of the halite cemented areas. The patchy compaction texture is suggestive of burial with a different, partial, pattern of cementation to the current one. What is certain, is that for most samples, the halite cement in its current distribution cannot have been the only control on the degree of compaction in the BSF.

Table 3: Modal analysis results from AQM, including minus cement quantification.

WELL	Depth (m)	Sample number	Total area analysed for PIA and AQM (mm^2)	Porosity from PIA	Normalised modal areas (%), excluding porosity, from AQM											Porosity = secondary	Area of cement representing grains	Minus cement porosity (%)	Theoretical porosity at current depth**	Maximum burial (m)*	Theoretical porosity at max burial depth**	Maximum burial pre- or post-Chalk*	Stratigraphy^	Gas / Water leg
					Quartz	K-feldspar	Plagioclase	Calcite	Dolomite	Anhydrite	Barite	Halite	Matrix / grain-coating clays	Micas	Kaolinite	Accessories									
41/18- 1	**511.00**	SSK16097	97	13.6	56.1	8.4	17.5	Tr	7.5	0.6	-	0.4	8.4	0.2	-	0.8	Tr	3.8	17.8	38.4	2764	23.6	Pre	VCS 2 mid	W
42/25-	**1137.30**	SSK7150	89	15.5	44.4	10.6	13.9	11.3	3.1	0.1	Tr	Tr	15.1	1.19	-	0.38	4.3	2.8	21.3	34.3	2133	27.7	Pre	VCS 1 top	W
	1142.48	SSK7151	108	13.8	41.8	7.6	9.2	28.9	3.2	0.5	0.1	Tr	7.8	0.4	-	0.5	Tr	21.4	23.7	34.3	2138	27.7	Pre	VCS 1 top	W
43/12- 1	**1388.52**	SSK16098	170	1.9	38.1	7.0	4.9	Tr	10.3	7.5	Tr	27.1	3.7	0.1	-	0.2	Tr	11.1	35.8	32.6	2287	26.7	Post	VCS 2 mid	W
	1391.87	SSK16099	129	27.6	50.1	9.1	21.9	0.1	4.4	0.1	-	1.2	11.3	0.5	-	1.3	Tr	2.2	30.4	32.6	2290	26.7	Post	VCS 2 mid	W
	1428.75	SSK16101	199	3.0	43.0	9.6	2.7	12.5	Tr	Tr	0.2	27.3	3.4	Tr	-	0.2	3.0	6.8	33.2	32.4	2327	26.4	Post	LVS 1 top	W
44/23- 3	**1374.80**	SSK7137 sandstone	16	21.9	42.6	7.5	11.0	0.1	24.2	4.1	-	-	8.7	0.1	0.4	0.6	Tr	21.8	29.1	32.7	1716	30.5	Post	VCS 2 mid	G
	1431.04	SSK7148	60	11.5	49.0	9.3	6.3	Tr	3.2	23.4	Tr	Tr	8.1	0.1	Tr	0.5	Tr	7.2	28.6	32.4	1772	30.1	Post	VCS 3 base	G
	1442.47	SSK7149A	171	22.5	58.2	16	5.4	Tr	2.3	12	Tr	-	5.8	Tr	Tr	0.1	1.0	2.3	30.3	32.3	1784	30.0	Post	LVS 1 top	W
44/23a- 10	**1855.30**	SSK7142	200	Tr	33.8	6.2	10.3	Tr	15.5	8.2	0.1	19.0	6.3	0.1	0.1	0.5	-	13.7	29.1	29.6	2095	28.0	Post	VCS 2 mid	G
	1918.23	SSK7134	115	11.2	64.4	9.1	1.6	Tr	0.1	0.4	-	21.6	2.7	Tr	0.1	0.1	0.5	0.5	30.0	29.1	2158	27.6	Post	LVS 1 top	W
	1921.60	SSK7135	123	22.6	56.0	14.9	3.2	19.5	0.9	Tr	Tr	0.5	4.8	Tr	Tr	0.1	1.0	7.8	32.3	29.1	2161	27.5	Post	LVS 1 top	W
48/10c- 11	**2016.56**	SSK16116	122	7.0	21.1	2.3	3.0	3.6	58.7	Tr	-	1.2	9.1	0.2	-	0.6	6.0	>20	N/A	28.5	3297	20.0	Equal	VCS 2 mid	W
	2080.87	SSK16110	167	2.0	62.6	5.2	0.3	2.4	-	0.9	-	26.8	1.6	Tr	-	0.1	2.0	2.3	27.3	28.1	3362	19.6	Equal	LVS 1 top	W
	2100.68	SSK16111	295	16.8	53.1	12.9	5.3	14.2	0.1	0.1	0.1	6.0	7.5	0.3	-	0.4	Tr	7.4	27.9	27.9	3381	19.5	Equal	LVS 1 top	W

* - from Bulat and Stoker 1987 ** - from Ramm and Bjorlykke, 1994, ^ - VCS – Volpriehausen Clay-Siltstone, LVS – Lower Volpriehausen Sandstone.
N/A – not applicable – sample is a dolocrete, value of minus cement porosity could not be reliably quantified.

4.3.2 Framework grain dissolution

Framework dissolution can be split between silicates and carbonates. Throughout the study area evidence for the minor to extensive dissolution of silicate framework grains was observed, primarily of felsic lithic fragments and feldspar grains. Plagioclase feldspars were noted to have been more significantly affected by dissolution than K-feldspars. Secondary porosity from this dissolution is highly varied, and largely minor (<2%, estimated), but in some samples contributes significantly to the total porosity (e.g. 48/10c- 11, 2016.6 m; Table 3).

Carbonate spherulitic nodules are framework grains; some have clear reworked textures and many occupy framework positions in the fabric of the sandstones. Dissolution and replacement of these is indicated by the presence of identifying concentric patterns of hematite-stained clay and silt within patches of neoformed cements, particularly in halite and anhydrite, but also in dolomite and calcite. These are instances of the primary (eodiagenetic) carbonate having been replaced and / or dissolved with the secondary porosity being recemented. Rarely residual primary carbonates with the associated clays and silt provide evidence of minor secondary porosity.

4.3.3 Diagenetic cement dissolution

Identification of dissolution textures in anhydrite is complicated by its common lath-terminated growth form, which is more obvious when seen in topographic imaging modes, appearing as an ‘etched’ margin when viewed in section. With this in mind, clear evidence for anhydrite dissolution is rare.

Identification of dissolution features in halite, and its timing, within this sample set is complicated by the uncertain storage history of the cores sampled as part of the study. Similarly, some of the halite observed may also be due to precipitation from residual brines or remobilisation of existing halite during the storage history.

5 Discussion

5.1 PARAGENETIC SEQUENCE

The principal diagenetic features and relative diagenetic chronology derived from this study in the Bunter Sandstone Formation are summarised schematically in Figure 15.

Our depositional model for the Bunter Sandstone is consistent with that of previous studies (Fine, 1986; Bifani, 1986; Ritchie and Pratsides, 1993; Purvis and Okkerman, 1996, Mckie and Williams, 2009) that suggest the BSF largely comprises fluvial / sheetflood deposits laid down in arid to semi-arid continental conditions. We have identified an aeolian input that increases in abundance eastwards, towards the top of the LVS, and in the base and middle of the VCS. The identification of possible pedogenic textures is also consistent with a model of periods of quiescence between occasional episodes of heavy rain.

One of the main complicating factors in determining the paragenetic evolution of the BSF that we have recognised in this regional study, is that the diagenetic cements are multi-episode, with periods of formation, replacement, and dissolution for the main cements (carbonates, sulphates and halite). These are locally variable in content and extent, so at any one site, evidence may only represent part of the story. The broad range of published models for the BSF paragenetic evolution from the basin illustrates this, as reviewed above.

Several eodiagenetic phases and textures recognised in this study point to evaporitic conditions being common throughout the deposition of both sandstones and mudstones, including expanded grain textures and the formation of calcrete and dolocrete nodules (sometimes referred to as 'cornstones') and laminations / beds, and nodular and enterolithic sulphates (gypcrete). Of particular note are the carbonate nodules, locally a major framework grain constituent, which we have identified as bearing concentric formation textures consistent with two formation mechanisms; local reworking and periodic in situ subsurface growth interspersed with infiltered hematitic clay pellicle development. Similar nodules have been recognised in the onshore equivalent Sherwood Sandstone Group (Burley, 1984; Strong and Milodowski, 1987; Plant *et al.*, 1999; Monaghan et al., 2012). There is a widespread recognition of calcrete and dolocrete horizons, and their localised reworking, in the BSF (e.g. Fine, 1986; Muir et al., 1994; Horning and Aigener, 1999; Blackbourn and Robertson, 2014). However, the carbonate nodules themselves, their importance as framework constituents and their evolution through eodiagenesis, are generally not well described in most published petrographic studies for the UKSNS (although Fine, 1986, does give a description of 'ooids' that are similar in many ways to our observations, for an onshore Denmark context). It seems likely that Blackbourn and Robertson (2014) have mis-identified them as all being reworked Bunter Shale ooids in their study (although we observed a few candidates for this origin (Figure 6G)). The $\partial^{18}O$ and $\partial^{13}C$ values (- 3.7 to -9.3‰PDB and -3.0 to +2.9‰PDB, respectively) for dolomite cement reported by Purvis and Okkerman (1996) support an early, near surface evaporitic origin for this carbonate in their study area, which concurs with paragenetic interpretation from our petrographic observations. Similarly, Muir et al. (1994) propose a shallow subsurface origin for some of the anhydrite, since Sr isotope data indicate a significant meteoric input, which fits our proposal for eodiagenetic sulphate in which anhydrite has formed both as a primary phase or through replacement of gypsum. Spain and Conrad (1997) also suggest early dolomite and anhydrite cementation controlled by palaeowater-table variability. Early anhydrite is also supported by anhydrite cementation excluding other cements (Purvis and Okkerman, 1996) and low levels of compaction (Muir et al., 1994). The majority of the anhydrite cement isotopic values ($\partial^{34}S$ +4.2 to +12.1‰ CDT) obtained by Purvis and Okkerman (1996), matched those of the underlying Zechstein evaporates, suggesting an external source for the sulphate. However, they had no evidence for early gypsum in their study, so it is likely that their isotopic evidence is related to mesodiagenetic anhydrite that has partially formed replacively, rather than primary eodiagenetic sulphate formation.

The timing of the halite cementation and the possibility of dissolution episodes as well as multiple sulphate cementation periods is where previous studies mainly differ in their conclusions. This is perhaps not surprising since minerals such as anhydrite and halite, which form major cements, are extremely soluble and potentially can be readily mobilised and redistributed by the movement of formation fluids at different times during the burial history. Halite cementation has largely been described as a late cement phase (Poroperm-Geochem, 1987; Laier and Nielsen, 1989; Van Bergen and De Leeuw, 2001). In some cases it is described as forming at least partially post hydrocarbon emplacement since halite appears inhibited in the gas leg (Ritchie and Pratsides, 1993; Poroperm-Geochem, 1987). These last observations are likely to be pre-gas emplacement local variations rather than a regional control; their deductions are contradicted by observations in this study that show halite also being well developed in some gas legs (43/15-B1, 44/23- 3, 44/23a- 10).

Other authors have recognised halite as an early cement (Muir et al., 1994; Purvis and Okkerman, 1996), with the latter noting that the halite infilled pores with no other cements. Whilst our own observations place halite as a paragenetically late phase, our high minus-cement porosity values

and observations of heterogeneous compaction textures are consistent with widespread pore-filling cements that were developed prior to significant burial. Texturally, our evidence supports the authors proposing early cementation models. Despite the different burial histories (Japsen, 2000; Bulat and Stoker, 1987) we see this pattern of early and extensive cementation across most of the study area; the only exception is the western edge (the samples from Quadrant 41). This supports the suggestion that major cementation pre-dated the periods when burial histories significantly diverged, i.e. before the Mid – Late Triassic onset of halokinesis and pre-Chalk uplift.

There are several different proposed origins of the halite, including high salinity ground waters (Muir et al., 1994), the underlying Zechstein (Purvis and Okkerman, 1996; Van Bergen and De Leeuw, 2001), or indeed both the overlying Haisborough Group and the Zechstein (Poroperm-Geochem, 1987). The current study is unable to add to this debate and recognises that additional work (isotopic) is required to inform further. However, we note that Purvis and Okkerman's (1996) hypothesis is backed by isotopic evidence from associated anhydrite and overall this model seems most likely for the earliest widespread halite cementation. With the evidence presented here and by other authors of several episodes of formation of both anhydrite and halite, including episodes of dissolution and replacement, multiple sources are likely for these major mesodiagenetic cements.

Together with a number of authors, we have observed a distribution of halite, and to a certain extent anhydrite, that is preferentially developed in coarser grained sandstones (Ketter, 1991; Poroperm-Geochem, 1987; Purvis and Okkerman, 1996). This is apparent both at a localised, individual lamination scale (e.g. Well 44/23a- 10, 1855.30 m; Well 48/10c- 11, 2130.86 m) and on a larger, bedding to Member scale. Halite is not seen as a major cement in samples that are dominantly of very fine sandstone. Most of the sandstones with abundant halite and all of the samples with complete halite cementation are fine, medium and coarse grained. However, not all of the coarser grained sandstones are significantly halite cemented showing that it is not grain size alone that controls the halite distribution. The mesodiagenetic anhydrite is also locally preferentially developed in coarser grained laminations, including in samples that are completely cemented by later halite (e.g. Well 43/12- 1, 1388.52 m). This 'reservoir quality inversion' phenomenon appears to be a feature across much of the BSF, suggesting cementation resulting from an influx of brines during burial, rather than *in situ* evaporative formation. The existence of a permeability control on brine movement and cementation is implicit in this observation.

Within the BSF, the LVS has the highest proportion of samples well-cemented by anhydrite and by halite. This reflects the overall coarser grain sizes that sandstones from this Member have; given that the grain size relationship with these cements is shown at a lamination scale, it is most likely that this is the determining factor rather than stratigraphic or depositional ones.

When considering halite cementation in samples just from the VCS Member, there is an additional depth relationship independent of grain size variation. Whilst some halite is present through the entire depth range of the study area (~500 m to ~2000 m), major halite cement is only present at and below a current burial depth of ~1400 m. This suggests that the halite distribution must be, in part, controlled by current and / or recent conditions. This current burial depth control on halite development suggests a modification on its distribution that fits the more recent models of Dingwall et al. (2013), and Blackbourn and Robertson (2014) relating to partial dissolution of cements due to meteoric influx from the BSF outcrop at the crest of a salt diapir to the east of the study area (Figure 1). Not all of the partially cemented intervals display evidence of dissolution, however, so if there were a widespread halite dissolution event there has also been subsequent new formation of halite.

Careful consideration is needed when attributing the origins of porosity created by halite dissolution. Some halite has formed in place of anhydrite. Both anhydrite and halite have locally replaced carbonates (both nodules and early cements). Consequently, high porosities identified where halite has been removed actually represent porosity after halite, sulphate and carbonate. Further, as the nodular carbonates are largely framework grains, then their replacement represents secondary porosity not restored primary porosity.

A striking feature of the BSF across the study area is the general absence of significant levels of diagenetic silicate cements. The only exceptions to this are samples from the western edge of the study area (near-shore well 41/18- 1) where compaction textures are well developed and quartz cement is widespread. Whilst this part of the study area has experienced the greatest uplift (>2200 m; Day, 1981; Bulat and Stoker, 1987; Japsen, 2000), its maximum burial is not the greatest in the area (Table 3), so this difference in compaction and silicate cement development is likely an indication that the degree of early pore-filling cementation was much lower than in the rest of the area, allowing silicate overgrowths to develop.

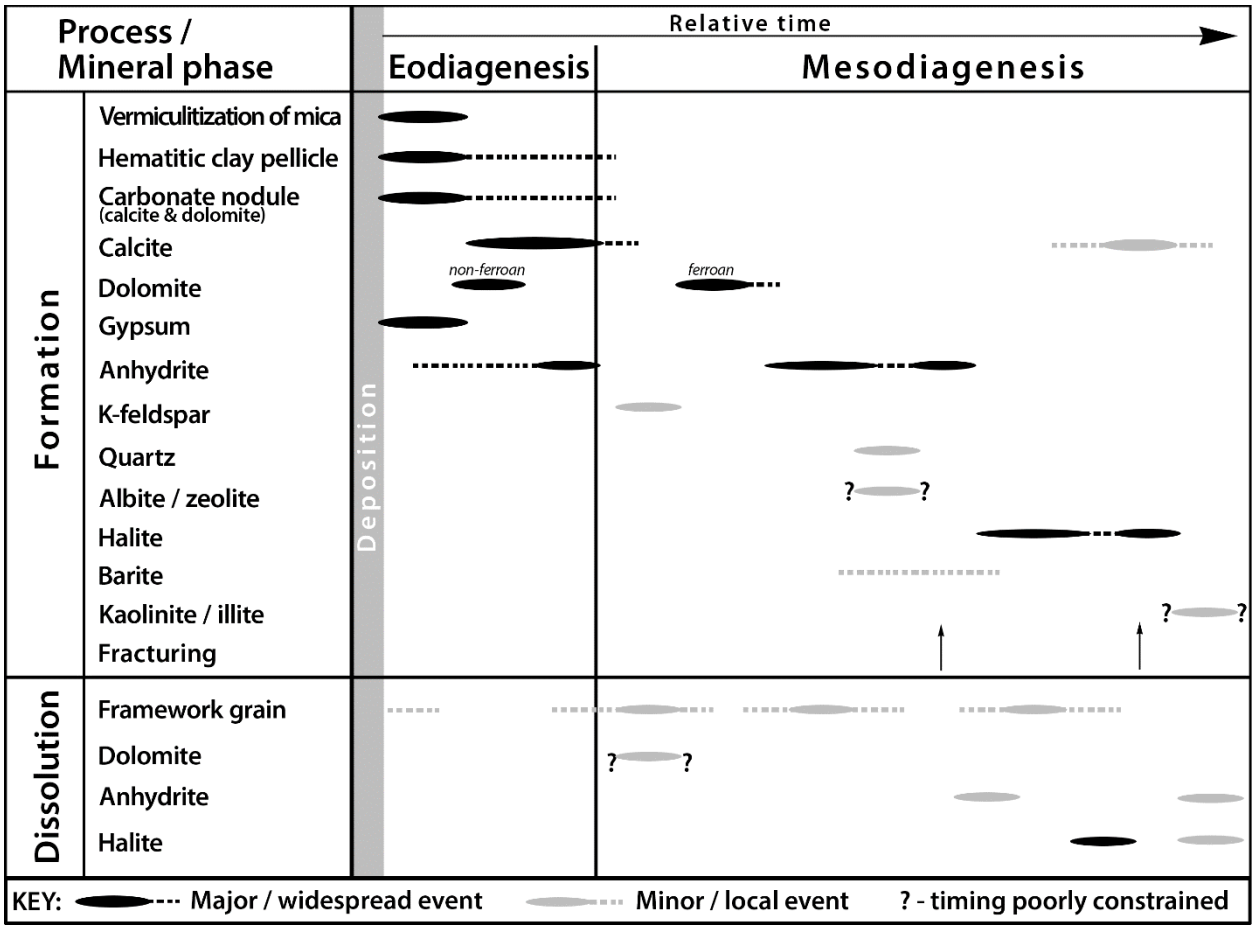

Figure 15: Paragenetic sequence for the Bunter Sandstone Formation in the UKSNS.

5.2 DISTRIBUTION AND TIMING OF CEMENTS RELATIVE TO BURIAL

As previously noted, the UKSNS basin has gone through episodes of burial and uplift since the deposition of BSF, resulting from a mix of regional basin tectonics and local halokinesis, locally resulting in exhumation of the BSF at the current sea floor. This is relevant because the timing of significant pore-filling cements can commonly be determined from textural observations in the

cemented areas (compaction, minus-cement porosity) combined with knowledge of regional and local burial histories. As noted in Section 1.1, for the BSF in the study area this is complicated by the complex history of burial and uplift that has affected different parts of the North Sea Basin. The most significant events in this context are continued burial post sedimentation through to the end of the Jurassic, when significant uplift occurred into the Cretaceous, followed by another period of significant burial during which the Chalk was deposited. Post-Chalk, further uplift occurred (earliest Palaeogene, also Neogene). Halokinesis is thought to have started Mid to Late Triassic and will have continued to create uplift patterns locally overprinting these regional trends. Consequently, there are no straight-forward burial histories that can be used interpretively over the whole study area. Simplifying, however, we can say that for most of the study area, maximum burial occurred during the post-Chalk burial, whilst for a few wells maximum burial occurred pre-Chalk (41/18- 1, 41/20- 1, 42/25- 1, 47/05- 1). For a couple of wells maximum burial depths were similar either side of the Chalk (48/10c- 11 and 43/16- 1). Halokinetic-related uplift may have locally disrupted these regional trends, and the inherent uncertainty of the timing of halokinesis, is a complicating factor in determining the timing of the main mesodiagenetic cements for the BSF relative to the episodes of burial and uplift, and therefore the controls on compaction.

6 Conclusions

This study has looked at the BSF in the southern North Sea through the petrographic analysis of 83 samples across 12 wells, with the aim of understanding its depositional and diagenetic histories, and characterising its present properties. With this information on a regional basis, an expected outcome is an improved ability to predict reservoir characteristic variations. The main conclusions are:

- The observed detrital and eodiagenetic characteristics of the BSF are consistent with terrestrial deposition under arid conditions, principally with fluvial origins, but with some input of aeolian grains, identifiable as well-rounded grains compared to the dominant sub-rounded to sub-angular grain shapes.
- Aeolian grain content is highest in the eastern part of the study area, and stratigraphically in the top of the LVS, and from the base and middle of the VCS.
- Diagenetic phases and cements are common to abundant through the BSF, marked by early (near-surface) carbonate and sulphate cements, with later sulphates and then halite. Some sandstones are completely cemented by diagenetic phases, others have high porosities with negligible diagenetic cements.
- An arid depositional environment is indicated by the identification of cements and nodular forms (carbonate and sulphate) that have developed at and near the depositional surface, some with evaporitic textures (e.g. pseudomorphed ‘desert rose’ forms, enterolithic anhydrite). The main evidence for near-surface formation is textural, including preserved un-compacted and expanded (displaced) grain frameworks.
- Carbonate nodules (calcite and dolomite) are an abundant framework grain constituent throughout the BSF. These are characterised by dominantly rounded sand sized forms with concentric structures defined by sequential zones of micritic and/or radial fibrous carbonate, and hematitic clays. Nodule cores comprise a mix of silt-grade silicate grains, mixed micrite and clays, and nodule fragments with evidence of varied degrees of reworking. They are most abundant in wells from the central to eastern parts of the study area (Quadrants 43 and 44).
- Carbonate nodules are locally concentrated in laminations, together with abundant eodiagenetic cements, forming dolocrete and calcrete layers of less than millimetre scale to more than centimetre scale thickness, with variable lateral continuity (dictated by the structure of the sedimentary laminations). Calcrete and dolocrete laminations are commonly, but not only, developed in finer grained laminations. These carbonate-cemented horizons are likely to present partial barriers to larger scale porosity interconnectivity and are at sub-seismic-resolution scales.
- The common framework positions of the carbonate nodules in sandstone fabrics might be mistaken (as in some earlier studies) as evidence for a purely detrital origin (i.e. as ooids). However, there is abundant and widespread evidence that they formed through both surface and shallow sub-surface processes, potentially with several periods of development, shallow burial, mobilisation and re-deposition. The commonly associated localised ‘expanded’ framework textures indicate growth in the sediment under minimal overburden. Some subsurface formation is also supported by radial crystal structures. The concentric layers of hematitic clay in this model mark episodic carbonate growth, with the clay layers either accumulating during periods of sediment mobilisation (i.e. as inherited clays) or through infiltration in near surface conditions. These are modes of clay coating development recognised for other framework grain types.

- The primary carbonate mineralogy of the nodules was calcite and dolomite. Primary mineralogy is variably preserved, with eodiagenetic replacement and recrystallisation by both dolomite and calcite, common. There is also widespread evidence for complete replacement by later mesodiagenetic cements (anhydrite, halite, albite).
- These eodiagenetic nodules are widespread throughout the study samples and strongly resemble features from the onshore equivalent of the BSF (cf. Burley, 1984; Strong and Milodowski, 1987; Plant et al., 1999; Monaghan et al., 2012). These early carbonate fabrics are typical of pedogenic cements.
- Anhydrite and gypsum are also eodiagenetic phases, with gypsum identified through pseudomorphic forms. In the sandstones there are finely crystalline sub-millimetre nodules with expanded grain textures indicating shallow sub-surface development. In the mudstones, anhydrite is commonly found as scattered concretions or nodules several tens of millimetres in diameter. They are particularly well-developed within the Intra-Solling Sand and Solling Claystone members.
- Several episodes of widespread and locally abundant anhydrite and halite mesodiagenetic cementation have been identified. These are generally poikilotopic cements, which in the case of anhydrite, differentiates it from the eodiagenetic nodules. Anhydrite largely pre-dates halite. Enclosure of anhydrite by halite is largely passive (i.e. anhydrite crystals have euhedral margins), but there is local evidence for dissolution of anhydrite prior to, or during, halite emplacement.
- Diagenetic silicate cements are rare over most of the study area, comprising minor quartz and K-feldspar overgrowths. The only exceptions to this are samples from the western edge of the study area (Quadrant 41 wells) where compaction textures are well developed and quartz cement is widespread. Other diagenetic phases are minor constituents, but include barite (poikilotopic, locally replacing anhydrite), kaolinite, fibrous illite, albite (locally replacing carbonate nodules) and zeolite.
- There is an observed grain size relationship with halite and anhydrite cement distributions in the sandstones, with both cement phases being preferentially developed in coarser sandstones.
- Locally, halite dissolution has occurred preferentially along coarser grained sandstone laminations in otherwise fully cemented intervals.
- Major halite cement is only present at and below a current burial depth of ~1400 m. This suggests that the halite distribution must be, in part, controlled by current and / or recent conditions.
- The legacy nature of the samples, means that some of the dissolution and precipitation features observed may be a consequence of post-coring effects, particularly small-scale halite and anhydrite dissolution, and pore-riming halite formation.
- A feature that is observed throughout the sandstones is a millimetre-scale heterogeneity in the degree of compaction observed across the study area and in all Formation Members. Areas of well compacted framework grains (long edge and sutured contacts, compaction-related grain fracturing and deformation) exist next to areas with more open (point contacts) and expanded fabrics. The looser textures can only partially be explained by grain replacement and the current distribution of cements (e.g. some anhydrite). We conclude that the samples were partially cemented prior to maximum burial, but the cement distribution has changed subsequently.
- The halite and anhydrite cements in their current distribution cannot have been the primary control on the degree of compaction in the BSF.

Our proposed diagenetic model infers that the sandstones had abundant, but not complete, early cements that preserved shallow framework fabrics. As these cements were partial, compactional fabrics were created in the surrounding less- or un-cemented zones. Subsequent dissolution, replacement and / or mobilisation of some or all of the cement phases, post maximum burial, has resulted in the widely recognised heterogeneous compaction fabric which does not correspond to current cement distributions. Since both anhydrite and halite show evidence for both multiple phases of formation and partial dissolution, these are the primary candidate minerals for dissolution / mobilisation. As these phases have also partially replaced some of the framework carbonate nodules, then their subsequent dissolution / mobilisation could also create an apparently uncompacted fabric.

One expected outcome of abundant, pre maximum burial cementation, is that Bunter Sandstone porosities should be detached from a simple linear variation with maximum burial depth. This is what is observed for petrographically calculated minus-cement primary porosities where determined. They are in most cases similar to estimated theoretical porosities at the current burial depth. It is recognised that the sample set is small and uncertainties in minus cement determination are high due to the abundant diagenetic cement and complex sequence of carbonate nodule formation and alteration / replacement.

An additional limitation of the study is that all samples have come from hydrocarbon industry boreholes, which have targeted potential reservoir structures. Many of these structures are a consequence of site-specific halokinesis, therefore with potentially atypical thermal, fluid and structural conditions.

Whilst we have gained significant insight into the diagenetic paragenesis, we are unable to adequately predict porosity, a major interest for CO_2 and energy storage interests. This is a consequence of the heterogeneities of the BSF in texture, cement distribution and paragenesis. To improve the remaining knowledge gaps and predictabilities of major reservoir properties, further studies are needed.

1. To obtain a better understanding of the distributions of grain fabrics and diagenetic cements, to improve predictability of pore size and connectivity, and porosity distribution at a regional scale:
    - Extend the study to include more samples for detailed modal analysis and minus cement porosity calculation.
    - Apply PIA to more samples and a wider range of properties to characterise actual porosity, grain size and compactional fabric distributions.
2. Develop a high-resolution diagenetic sequence through isotopic studies of the main cements, tied to their paragenetic sequencing using:
    - Strontium isotope analysis ($^{87}Sr/^{86}Sr$) to inform the origins of solutes in the diagenetic fluids, and extent of rock-water interaction, related to diagenetic mineral formation episodes. The laser ablation – inductively coupled plasma – mass spectroscopy (LA-ICP-MS) analysis technique with a spatial resolution of 100 µm can potentially be used for this purpose, to micro-sample discrete diagenetic cement components (target phases - calcite, dolomite, anhydrite and halite).
    - Stable (oxygen, carbon, sulphur) isotope analysis ($\delta^{13}C$, $\delta^{18}O$ and $\delta^{34}S$). These techniques would further inform the mineralisation temperature, and carbon and sulphur sources as well the geochemical processes involved in the development of the target phases - anhydrite, dolomite and calcite cements.
    - U-Pb dating to obtain absolute dates for carbonate mineral formation. Using petrographically-guided targeting, this will place the paragenetic sequence in absolute

time. A major issue for this will be potential contamination of the carbonate phases by finely disseminated hematite, which is known to preferentially concentrate U and Pb.

The expected outcomes, on a regional basis, would be:

- A higher resolution understanding of the distributions and variations in grain size, grain fabric, cements, porosity and pore interconnectivity, of the BSF. These would be targeted to link in to other datasets for improved BSF property predictions.
- Absolute dates for episodes of carbonate growth already placed in a relative time paragenetic sequence by detailed petrography.
- Stable and radiogenic isotope data that will be used to inform the origins of the fluids related to all of the main cement phases, as well as for the dated mineral formation episodes.
- Combine these data with existing petrographic datasets to create an integrated knowledge of the development of pore-scale fluid-flow, compaction, and cementation on an actual (rather than relative) time scale.

7 Appendix 1

Summary spreadsheet, containing original petrographic data, available on request.

References

British Geological Survey holds most of the references listed below, and copies may be obtained via the library service subject to copyright legislation (contact libuser@bgs.ac.uk for details). The library catalogue is available at: https://envirolib.apps.nerc.ac.uk/olibcgi.

OIL AND GAS AUTHORITY. 2021. Carbon dioxide appraisal and storage licences. [cited 29 July 2021]. Available from https://www.ogauthority.co.uk/licensing-consents/carbon-storage/

UK GOVERNMENT. 2019. UK becomes first major economy to pass net zero emissions law. [cited 29 July 2021] Available from https://www.gov.uk/government/news/uk-becomes-first-major-economy-to-pass-net-zero-emissions-law published 27 June 2019.

THE ENERGY TECHNOLOGIES INSTITUTE LLP. 2021. CO_2 Stored CO_2 Storage Evaluation Database Version 2 Release 1. [cited 29 July 2021] Available from http://www.co2stored.co.uk/

BACHMANN, G H, Geluk, M C, Warrington, G, Becker-Roman, A, Beutler, G, Hagdorn, H, Hounslow, M W, Nitsch, E, Rohling, H-G, Simon, T, and Szulc, A. 2010. Triassic. 149–173 in *Petroleum Geological Atlas of the Southern Permian Basin Area* DOORNENBAL, J C, and STEVENSON, A G. (editors). (Houten: EAGE.) ISBN 9789073781610

BATH, A H, MILODOWSKI, A E, and STRONG, G E. 1986. Fluid flow and diagenesis in the East Midlands Triassic sandstone aquifer. 127–140 in *Fluid Flow in Sedimentary Basins and Aquifers*. GOFF, J C, and WILLIAMS, B P J. (editors). (London: Geological Society Special Publications.) Vol. 34, ISBN 0 632 01804 6

BATHURST, R G C. 1975. *Carbonate Sediments and their Diagenesis*. Developments in Sedimentology, Vol. 12. 2nd enlarged edition (Amsterdam: Elsevier.) ISBN 9780444413536

BENTHAM, M. 2006. An assessment of carbon sequestration potential in the UK – Southern North Sea case study. Tyndall Centre for Climate Change Research, Working Paper 85.

BIFANI, R. 1986. Esmond Gas Complex. 209–221 in *Habitat of Palaeozoic Gas in N.W. Europe. Geological Society Special Publication No. 23*. BROOKS, J, GOFF, J C, and VAN HOORN, B. (editors). (Edinburgh: Scottish Academic Press.) ISBN 7073 0491 1

BLACKBOURN, G A, and ROBERTSON, L F. 2014. Sedimentology, petrography and burial history of the cored Triassic section in the National Grid Carbon well 42/25d-3, UK North Sea. *Blackbourn Geoconsulting.* Available from the National Data Repository, https://ndr.ogauthority.co.uk/.

BRADEAU, E, ASSI, A T, BOUKCIM, H, and MOHTAR, R H. [2014]. Physics of the soil medium organization part 1: thermodynamic formulation of the pedostructure water retention and shrinkage curves [online]. *Frontiers in Environmental Science*, Vol. 2(4). Available from https://doi.org/10.3389/fenvs.2014.00004

BULAT, J, and STOKER, S J. 1987. Uplift determination from interval velocity studies, UK southern North Sea. 293–305 in Conference on *Petroleum Geology of North West Europe*., 3rd, 1986. BROOKS, J, and GLENNIE, K W. (editors) (London: Graham & Trotman.)

BURLEY, S D. 1984. Patterns of diagenesis in the Sherwood Sandstone Group (Triassic), United Kingdom. *Clay Minerals*, Vol. 19, 403–440.

BUTLER, G P. 1969. Modern evaporite deposits and geochemistry of coexisting brines, the sabkha, Trucial coast, Arabian Gulf. *Journal of Sedimentary Petrology*, Vol. 39, 70–78.

CAMERON, T D J, CROSBY, A, BALSON, P S, JEFFERY, D H, LOTT, G K, BULAT, J, and HARRISON, D J. 1992. United Kingdom offshore regional report: *the geology of the southern North Sea*. (London: HMSO for the British Geological Survey.) ISBN 0 11 884492 X

DEAN, W E, DAVIS, G R, and ANDERSON, R Y. 1975. Sedimentological significance of nodular and laminated anhydrite. *Geology*, Vol. 3, 367–372.

DINGWALL, S, FURNIVAL, S, WRIGHT, S, and MORRISON, D. 2013. Integrated subsurface evaluation of a saline aquifer selected for CO_2 disposal. 75th EAGE Conference and Exhibition. 10–13 June 2013.

DOORNENBAL, H, AND STEVENSON, A. (editors). 2010. Petroleum Geological Atlas of the Southern Permian Basin Area. EAGE, Houten, The Netherlands.

FINE, S. 1986. The diagenesis of the Lower Triassic Bunter Sandstone Formation, Onshore Denmark, *Danmarks Geologiske Undersøgelse*. Serie A, Vol. 15, 1-15. https://doi.org/10.34194/seriea.v15.7034

FURNIVAL, S, WRIGHT, S, DINGWALL, S, BAILEY, P, BROWN, A, MORRISON, D, and DE SILVA, R. 2014a. Subsurface characterisation of a saline aquifer cited for commercial scale CO_2 disposal. GHGT-12, *Energy Procedia*, Vol. 63, 4926–4936.

FURNIVAL, S, BROWN, A, ROWBOTHAM, P, WRIGHT, I, and DE SILVA, R. 2014b. Planning for commercial scale CO_2 storage in a massive UK Saline aquifer. Don Valley CCS project.

GELUK, M C, and ROHLING, H-G. 1997. High-resolution sequence stratigraphy of the Lower Triassic 'Buntsandstein' in the Netherlands and northwestern Germany. *Geologie en Mijnbouw,* Vol. 76, 227–246.

GELUK, M C. 2005. Stratigraphy and tectonics of Permo-Triassic basins in the Netherlands and surrounding areas. Thesis for Universiteit Utrecht, The Netherlands. ISBN 90-393-3911-2

GRANT, R J, UNDERHILL, J R , HERNÁNDEZ-CASADO, J, RACHEL, JAMIESON, J, and WILLIAMS, R M. 2021. The evolution of the Dowsing Graben System: implications for petroleum prospectivity in the UK Southern North Sea. *Petroleum Geoscience*, Vol. 27, petgeo2018-064, 16 December 2019.

HEINEMANN, N, WILKINSON, M, PICKUP, G E, HASZELDINE, R S, and CUTLER, N A. 2012 CO_2 storage in the offshore UK Bunter Sandstone Formation. *International Journal of Greenhouse Gas Control*, Vol. 6, 210–219.

JAPSEN, P. 2000. Investigation of multi-phase erosion using reconstructed shale trends based on sonic data. Sole Pit axis, North Sea. *Global and Planetary Change* Vol. 24, 189–210.

JOHNSON, H, WARRINGTON, G, and STOKER, S J. 1994. Permian and Triassic of the southern North Sea. 33–51 in *Lithostratigraphic nomenclature of the UK North Sea.* KNOX, R W O B, and CORDEY, W G. (editors). (Nottingham: British Geological Survey for the UK Offshore Operators Association). ISBN 0 85272 224 9

KETTER, F J. 1991. The Esmond, Forbes and Gordon Fields, Block 43/8a, 43/13a, 43/15a, 43/20a, UK North Sea. 425–432 in *United Kingdom Oil and Gas fields, 25 Years Commemorative Volume, Geological Society London Memoir 14.* ABBOTTS, I L. (editor) (London: Geological Society London.) ISBN 0 903317 62 1

KINSMAN, D J CORDAY. 1969. Modes of formation, sedimentary associations and diagenetic features of shallow water and supratidal evaporates. *Bulletin of the American Association of Petroleum Geologists*, Vol. 53, 830–840.

KNOX, R W O'B, BURGESS, W G, WILSON, K S, and BATH, A H. 1984. Diagenetic influences on reservoir properties of the Sherwood Sandstone (Triassic) in the Marchwood Geothermal borehole, Southampton, U.K. *Clay Minerals*, Vol. 19, 441–456.

LAIER, T and NIELSEN, B L. 1989. Cementing halite in Triassic Bunter Sandstone (Tønder, southwest Denmark) as a result of hyperfiltration of brines. *Chemical Geology*, Vol. 76, 353-363.

MCHARDY, W J , WILSON, M J., and TAIT, J M. 1982. Electron microscope and X-ray diffraction studies of filamentous illitic clay from sandstones of the Magnus Field. *Clay Minerals*, Vol. 17, 23–39.

MCKIE, T, and WILLIAMS, B. 2009. Triassic palaeogeography and fluvial dispersal across the northwest European Basins. Geological Journal. Vol. 44, 711-741. DOI: 10.1002/gj.1201.

MILODOWSKI, A E; STRONG, G E; WILSON, K S; HOLLOWAY, S; BATH, A H; BRANCH, C H; SPIRO, B. 1987. Diagenetic influences in the aquifer properties of the Permo-Triassic sandstones in the East Yorkshire and Lincolnshire Basin. *Investigation of the Geothermal Potential of the UK.* British Geological Survey. Keyworth, Nottingham, UK.

MILODOWSKI, A E, GILLESPIE, M R, NADEN, J, FORTEY, N J, SHEPHERD, T J, PEARCE, J M, and METCALFE, R. 1998. The petrology and paragenesis of fracture mineralization in the Sellafield area, west Cumbria. *Proceedings of the Yorkshire Geological Society*, Vol. 52, 215–241.

MILODOWSKI, A E, and RUSHTON, J E. 2008. Mineralogical and porosity characterisation of potential aquifer and seal units for carbon capture and storage methodologies for the CASSEM Project. *British Geological Survey Report*, CR/08/153.

MILODOWSKI, A E, NORTHMORE, K J, KEMP, S J, ENTWISTLE, D C, GUNN, D A, JACKSON, P D, BOARDMAN, D I, ZOUMPAKIS, A, ROGERS, C D F, DIXON, N, JEFFERSON, I, SMALLEY, I J, and CLARKE, M. 2015. The mineralogy and fabric of 'Brickearths' in Kent, UK and their relationship to engineering behaviour. *Bulletin of Engineering Geology and the Environment,* Vol. 74. 1187–1211.

MONAGHAN, A, FORD, J, MILODOWSKI, A, MCINROY, D, PHARAOH, T, RUSHTON, J, BROWNE, M, COOPER, A, HULBERT, A, and NAPIER, B. 2012. 3D geological models of aquifer and seal rocks at analogue CO_2 storage sites in Lincolnshire and eastern Scotland, UK. *Proceedings of the Yorkshire Geological Society*, Vol. 59, 53–76.

MUIR, R O, THIRWALL, M, and WALSH, J N. 1994. The Upper Buntsandstein in well 49/6A-4. A sedimentological and geochemical investigation of the origins of the cements. Royal Holloway, University of London Report. Available from the National Data Repository, https://ndr.ogauthority.co.uk/.

PAXTON, S T, SZABO, J O, AJDUKIEWICZ, J M, and KLIMENTIDIS, R E. 2002. Construction of an intergranular volume compaction curve for evaluating and predicting compaction and porosity loss in rigid-grain sandstone reservoirs. *AAPG Bulletin*, Vol. 86(12), 2047–2067.

PETTIJOHN, F J, POTTER, O E, and SEIVER, R. 1987. *Sand and Sandstone*. (New York: Springer.) ISBN 978 1 4612 1066 5

PLANT, J A, JONES, D G, and HASLAM, H W. (EDITORS), 1999. *The Cheshire Basin: Evolution, Fluid Movement and Mineral Resources in a Permo-Triassic Rift Setting*. (Nottingham: British Geological Survey.) ISBN 0852723334

POROPERM-GEOCHEM LIMITED. 1987. Sedimentological and Petrological analysis of core from wells 44/23-3 and 44/23-5. Report number 1956, for CSX Oil and Gas (UK) Corp. Available from the National Data Repository, https://ndr.ogauthority.co.uk/.

PURVIS, K, and OKKERMAN, J A. 1996. Inversion of reservoir quality by early diagenesis: an example from the Triassic Buntsandstein, offshore the Netherlands. 179–189 in *Geology of gas and oil under the Netherlands.* RONDEEL, H.E., BATJES, D.A.J. and NIEUWENHUIJS, W.H. (editors) (The Hague: Kluwer Academic Publishers) ISBN 978 94 009 0232 6

NOY, D J, HOLLOWAY, S, CHADWICK, R A, WILLIAMS, J D O, HANNIS, S D, and LAHANN, R W. 2012. Modelling large-scale carbon dioxide injection into the Bunter Sandstone in the UK Southern North Sea. *International Journal of Greenhouse Gas Control,* Vol. 9, 220–233.

RAMM, M, and BJORLYKKE, K, 1994. Porosity/depth trends in reservoir sandstones; assessing the quantitative effects of varying pore-pressure, temperature history and mineralogy, Norwegian Shelf data: *Clay Minerals*, Vol. 29, 475–490.

RITCHIE, J S, PRATSIDES, P. 1993. The Caister fields, Block 44/23a, UK North Sea. 759–769 in *Petroleum Geology of Northwest Europe: Proceedings of the Fourth Conference*. PARKER J R. (editor). (London: The Geological Society.) ISBN 0 903317 85 0

ROSENFELD, M A. 1949. Some aspects of porosity and cementation. *Producers Monthly*, Vol. 13(7), 39–42.

RUFFELL, A., and HOUNSLOW, M. 2006. Triassic: seasonal rivers, dusty deserts and saline lakes. 295–325 in *The Geology of England & Wales*. RAWSON, P F, and BRENCHLEY, P. (editors) (London: The Geological Society of London) ISBN 9781862393882

SCHMIDT, V, and MCDONALD, D A. 1979a. The role of secondary porosity in the course of sandstone diagenesis. 175–207 in *Aspects of Diagenesis.* SCHOLLE, P A, and SCHLUGER, P R. (editors). Society of Economic Paleontologists and Mineralogists Special Publication, Vol. 26.

SCHMIDT, V, and MCDONALD, D A. 1979b. Texture recognition of secondary porosity in sandstones. 209–225 in *Aspects of Diagenesis*. SCHOLLE, P A, and SCHLUGER, P R. (editors). Society of Economic Paleontologists and Mineralogists Special Publication, Vol. 26.

SHEARMAN, D J. 1966. Origin of marine evaporates by diagenesis. *Transactions of the Institute of Mining and Metallurgy*, Vol. 75, 208–215.

SPAIN, D R and CONRAD, C P. 1997. Quantitative analysis of top-seal capacity: offshore Netherlands, southern North Sea. *Geologie en Mijnbouw*, Vol. 76, 217–226.

STRONG, G E, and MILODOWSKI, A E. 1987. Aspects of the diagenesis of the Sherwood Sandstones of the Wessex Basin and their influence on reservoir characteristics. 325–337 in *Diagenesis of Sedimentary Sequences*. MARSHALL, J D. (editor). Geological Society Special Publication, Vol. 36.

STRONG, G E, MILODOWSKI, A E, PEARCE, J M, KEMP, S J, PRIOR, S V, and MORTON, A C. 1994. The petrology and diagenesis of Permo-Triassic rocks of the Sellafield area, Cumbria. *Proceedings of the Yorkshire Geological Society*, Vol. 50, 77–89.

TESTA, G, and LUGLI, S. 2000. Gypsum-anhydrite transformations in Messinian evaporites of central Tuscany (Italy). *Sedimentary Geology*, Vol. 130, 249–268.

UNDERHILL, J R. 2003. The tectonic and stratigraphic framework of the United Kingdom's oil and gas fields. 17–59 in *United Kingdom Oil and Gas Fields, Commemorative Millennium Volume*. GLUYAS, J G, and HICHENS, H M. (editors) Geological Society, London, Memoirs, Vol. 20.

UNDERHILL, JR. 2009. Role of intrusion-induced salt mobility in controlling the formation of the enigmatic 'Silverpit Crater', UK Southern North Sea. *Petroleum Geoscience*, Vol. 15, 197–216.

VAN BERGEN, F, and LEEUW, C S. 2001. Salt cementation of reservoir rocks near salt domes in the Netherlands North Sea area – A new mechanism. EAGE 63rd conference and technical exhibition. 11-15 June 2001

WALKER, T R, WAUGH, B, and GRONE, A J. 1978. Diagenesis in first-cycle desert alluvium of Cenozoic age, southwestern United States and northwest Mexico. *Geological Society of America Bulletin*. Vol. 89, 19–32.

WEIBEL, R, and FRIIS, H. 2004. Opaque minerals as keys for distinguishing oxidising and reducing diagenetic conditions in the Lower Triassic Bunter Sandstone, North German Basin. *Sedimentary Geology*, Vol. 169, 129–149.

WILSON, M D. 1992. Inherited grain-rimming clays in sandstones from eolian and shelf environments: their origin and control on reservoir properties. 209–225 in *Origin, Diagenesis, and Petrophysics of Clay Minerals in Sandstones*. HOUSEKNECHT, D.W., and PITTMAN, E D. (editors). Society of Economic Paleontologists and Mineralogists, Special Publication Vol. 47.